

Preparation of bio-based powder for 3D printing applications by Selective Laser Sintering

Giorgio De Trane, s275514

November 14, 2022

POLITECNICO DI TORINO
Department of Mechanical and Aerospace Engineering



Master of Science in Aerospace Engineering

Supervisor: Prof. Massimo Messori
Co-supervisor: Prof. Giovanna Colucci

To my parents, whose love has always been unconditional, intense and at times
hard to comprehend.

Abstract

The goal of this case study is to optimize the production of SLS suitable fine powders of sustainable biopolymers and directly assess their printability.

Among the ~~bi~~ polymers, PLA is the most widely used in the *Fused Deposition Modeling* (FDM) hobbyist and enthusiast markets, whereas more invasive polymers such as PA12 are commonly used in *Selective Laser Sintering* (SLS), the most common 3D printing technology for the production of functional parts.

A higher demand for biopolymers in the SLS industry is expected in the near future - following the general sustainability goals of all industries - as the technology allows for the production of more complex geometries and intricate details, as well as ad-hoc parts for the medical industry, where the use of biopolymers is already widespread.

The catalogue of biopolymers available for SLS is currently expanding, but still limited, and the production of fine powders is a critical step in the process of producing functional parts.

This study focused on ~~P~~ BH, a copolymer of the *Polyhydroxyalcanoate* family, with a wider sintering window and thus a ~~hi~~ potential for SLS applications, compared to other polymers of the same group.

An extensive research on current *state-of-the-art* production methods, most notably cryogenic mechanical milling and chemical precipitation, led to choosing the latter, since the former does not produce spherical particles, unless further heat treatments are applied, with unpredictable rates of success and potentially high power consumption.

An initial recipe for PHBH, previously tested by other researchers, has been tweaked and improved, achieving over a ten-fold increase in *pellet-to-powder* yield, compared to the very early stages of production.

PHBH microspheres were obtained by oil-in-water emulsion solvent evaporation method.

The process involves the dissolution of the polymer in chloroform, followed by dripping the viscous liquid in a water solution containing 0.25 %_{wt} of PVA and stirring the mixture, which leads to the complete solvent evaporation and the polymer precipitation as a fine powder.

The resulting powder is then cleaned, dried overnight and sieved, to obtain a final product with a particle size distribution suitable for SLS applications (< 100 μm).

Specimens of the obtained powder have been collected and characterized by means of a series of tests, including various thermal analysis methods, such as TGA and DSC, as well as a flowability test and density measurements via a gas pycnometer.

 The SLS suitability of the powder has been further assessed in terms of morphology by *Scanning Electron Microscopy* (SEM), which revealed a close to ideal distribution of predominantly spherical, non-hollow particles, as also confirmed by granulometry investigations.

The powder has been printed on an SLS 3D printer, with single layer and multilayer objects achieving a print quality comparable to that of standard SLS polymers such as PA12.

Complex geometries and intricate details have been successfully printed as a proof of concept, as well as prismatic samples.

Contents

1 Thesis Goal	8
2 Introduction	9
2.1 Polymers in Additive Manufacturing	9
2.2 Common AM techniques for polymers	10
2.2.1 FDM (Fused Deposition Modeling)	11
2.2.2 SLS (Selective Laser Sintering)	12
3 PHAs (Polyhydroxyalkanoates)	14
3.1 PHA and Additive Manufacturing	15
3.1.1 PHBH	15
4 PBS (Polybutylene Succinate)	16
5 PBAT (Polybutylene Adipate Terephthalate)	17
6 Powder production for SLS	18
6.1 Powder requirements for SLS	18
6.2 Mechanical milling	19
6.3 Chemical precipitation	20
6.3.1 Polymer-Solvent System	20
6.3.2 Cloud point diagram	21
6.3.3 Production in a controlled environment	21
6.4 Environmental impact	21
7 Laboratory environmental conditions and available equipment	23
8 Choice of material and production process	24
9 Initial chemical precipitation recipe for PHBH	25
9.1 Components	25
9.2 Equipment	26
9.3 Detailed step-by-step reaction	27
9.4 Initial results and failures	31
10 Recipe tweaking and improvements	32
10.1 Key variables	32
10.2 Adaptations and progressively refined equipment choice	34
10.3 Current results	35
10.4 Consistent reproducibility and scalability	36
11 Powder granulometry and morphology	37
11.1 Sieving process	37
11.2 SEM (Scanning Electron Microscope) analysis	38
11.2.1 Results	40

12 Thermal analysis	48
12.1 DSC (Differential Scanning Calorimetry)	48
12.1.1 Results	48
12.2 TGA (Thermal Gravimetric Analysis)	54
12.2.1 Results	54
13 Density measurement	61
	
14 Flowability analysis	62
15 Granulometry analysis	63
16 SLS printing	66
16.1 Print files preparation	66
16.1.1 3D model creation	67
16.1.2 Slicing	68
16.2 Sharebot Snowwhite ²	70
16.3 Printed samples	73
17 Dynamic Mechanical Analysis	78
18 Future development and research	81

List of Figures

1	Phases of an <i>SLS</i> process [23, 5]	12
2	Schematic representation of the PHBH polymer structure [6, 23].	15
3	Two spherical powder particles forming a sintering neck [23]	18
4	Generic TEAS plot for any given polymer [7, 23]	20
5	Particle size decreases as stirring RPM increase [7, 23]	21
6	Process diagram [23]	27
7	A bulk preparation of PVA solution.	29
8	"Round particles seen through a SEM microscope" as imagined by Dall-E 2's artificial intelligence algohorithm [2, 3]	39
9	Example of a SEM image before and after enhancing [23, 28]	41
10	Enhanced SEM image, $SEM_{01} - 461X_{(SE1)}$ [28, 21]	42
11	Enhanced SEM image, $SEM_{02} - 461X_{(SE1)}$ [28, 21]	42
12	Enhanced SEM image, $SEM_{03} - 461X_{(SE1)}$ [28, 21]	43
13	Enhanced SEM image, $SEM_{04} - 461X_{(SE1)}$ [28, 21]	43
14	Enhanced SEM image, $SEM_{05} - 461X_{(SE1)}$ [28, 21]	44
15	Enhanced SEM image, $SEM_{06} - 461X_{(SE1)}$ [28, 21]	44
16	Enhanced SEM image, $SEM_{07} - 800X_{(VPSE\ G4)}$ [28, 21]	45
17	Enhanced SEM image, $SEM_{08} - 800X_{(VPSE\ G4)}$ [28, 21]	45
18	Enhanced SEM image, $SEM_{09} - 800X_{(VPSE\ G4)}$ [28, 21]	46
19	Enhanced SEM image, $SEM_{10} - 400X_{(VPSE\ G4)}$ [28, 21]	46
20	Enhanced SEM image, $SEM_{11} - 400X_{(VPSE\ G4)}$ [28, 21]	47
21	Enhanced SEM image, $SEM_{12} - 400X_{(VPSE\ G4)}$ [28, 21]	47
22	Mettler-Toledo DSC-1 STARe System [30]	49
23	DSC analysis of PHBH at $10\ ^\circ C/min$	51
24	Enthalpy values for the DSC analysis of PHBH at $10\ ^\circ C/min$	53
25	Mettler-Toledo TGA/SDTA 851e [30]	55
26	TGA analysis of pellet sample $P - TGA_{01}$ (4)	56
27	TGA analysis of powder sample $p - TGA_{02}$ (4)	57
28	TGA analysis of powder sample $p - TGA_{03}$ (4)	58
29	TGA analysis of sintered sample $s - TGA_{04}$ (4)	59
30	Ultrapyc 5000 gas pycnometer [20]	61
31	Malvern Morphologi 4 [22]	63
32	Granulometry analysis of the powder sample	64
33	SLS ready powder batch	66
34	3D printing file pipeline	67
35	Sharebot Snowwhite ²	70
36	Sharebot Snowwhite ² UI	71
37	First printing attempts. Porosity and defects are more visible in the single layer samples. The rectangular prisms were the first to showcase a good level of densification and lack of deformation and have been used as a baseline for the following tests.	74
38	From top to bottom, clockwise: 15— <i>dragonlogofilled</i> , 15— <i>hexagonfilled</i> , 55— <i>octagonholesthin</i> , 50— <i>boatthin</i> , 10— <i>DMA01filled</i> , 01— <i>squarefilled</i> (5).	75

39	Printed specimens used for DMA testing.	76
40	Printed specimens with complex internal patterns.	77
41	DMA analysis of the SLS sample 10 – <i>DMA01_{filled}</i> (5).	79

List of Tables

1	All catalogued SEM samples	40
2	DSC specimens	50
3	Results of the DSC analysis showcasing phase transition points, enthalpies and crystallinity of the material	53
4	TGA specimens	55
5	A list of the most relevant 3D printed specimens	75

1 Thesis Goal

The ever increasing demand for sustainable materials in all manufacturing industries has led to a growing interest in the production of biopolymers for various applications.

In particular, the interest for biopolymers in the Additive Manufacturing industry has skyrocketed in the last few years, along with the general interest in sustainable materials, and the use of biopolymers in 3D printing is expected to grow in the near future, with more research and resources being invested in the field, and costs decreasing as the market share increases.

Among the various AM techniques, *Selective Laser Sintering* (SLS) is increasing in popularity and maturing as a technology. This includes its applications with biopolymers themselves, which are already used in the medical industry, but are still limited in terms of the number of available polymers and the production of fine powders for SLS applications.

The current literature on the subject is still scarce and the available systematic reviews highlight the need for further research in the field, in order to expand the catalogue of biopolymers available for 3D printing and to optimize the production of fine powders for SLS specifically.

The goal of this case study is to further explore the production of biopolymer fine powders for SLS applications, with a focus on PHBH and chemical precipitation, by optimizing the production pipeline, characterizing and directly assessing the printability of the resulting powder.

2 Introduction

Additive manufacturing (AM) is a broad term that encompasses several manufacturing techniques, characterized by their additive nature, as the name suggests, in contrast with more traditional subtractive processes.

AM techniques are applied to a  range of materials, including ceramics, polymers and metal alloys, some of which are specifically developed or optimized to these kinds of applications.

The main advantage of AM is the ability to produce complex shapes in a relatively short time. These geometries are either too hard or even impossible to reproduce with subtractive manufacturing techniques, which often require multiple steps, using different pieces of equipment, trained personnel .

Given the same material, the complex shapes allowed by AM can replace components made of multiple assembled parts with a unique solid piece of comparable or even better mechanical properties.

The inherent flexibility of AM often allows product designers to simplify or even entirely bypass the very strict CAD workflow (which is inherently tied to traditional manufacturing processes) and make use of organic and/or generative modeling.

As a consequence of better design choices and minimal need of post-processing of AM objects, far less raw material is wasted, compared to subtractive manufacturing techniques, leading to long term lowering of costs, faster design-to-market pipelines and, last but not least, lower emissions and environmental impact [31]. 

2.1 Polymers in Additive Manufacturing

Polymers and their composite materials have been used in all sorts of fields, ranging from arts and crafts all the way to advanced biomedical and aerospace applications, thanks to their unique and varied extended range of properties. 

The rapid advancement of AM, where polymers have been extensively used for prototyping, in the form of resins, filaments, powders and viscous inks, has increased the demand for high-performance polymers, in order to take advantage of their quicker printing times (compared to metals) as well as their lower cost, while still maintaining good mechanical properties for an end product, rather than just a prototype [31].

The urge for drastically reducing the environmental impact of human activities involves every production field, including AM, which can be inherently less impactful than traditional manufacturing processes, given the same material and final product to achieve.

A consequence of the concerns about climate change and its potentially catastrophic outcomes is the research in the field of eco-friendly materials, including polymers that could be used in AM.

A good example is **PLA** (PolyLactic Acid), a polymer widely used in 3D printing, whose monomer is obtained by fermenting starches, such as corn starch.

Many new eco-friendly polymers have been and are currently being studied for AM techniques, but this case study will focus mostly on materials that can be potentially turned into powders for **PBF** (Powder Bed Fusion) techniques or filaments for **ME** (Material Extrusion).

2.2 Common AM techniques for polymers

Polymers can be processed with several AM techniques, including, but not limited to:

- **VP** (Vat Photopolymerization), which makes use of UV lights (or other radiations) to solidify photosensitive resins. This class of AM processes can produce parts with the highest resolution among all AM methods [31, 15];
- **MJ** (Material Jetting), which consist of a deposition of viscous fluids (either in droplets or in a continuous fashion), solidified by different agents (time interacting chemicals, heating, cooling, drying, photopolymerization, etc.). These processes include several patented methods, characterized by high speed printing [31];
- **PBF** (Powder Bed Fusion), where the object is printed by locally fusing a powder bed (with a pulsing energy source -such as lasers- or with a local deposition of chemicals), layed out in a layer-by-layer fashion [31, 15];
- **ME** (Material Extrusion), where each layer is printed by direct deposition of materials through a nozzle, that solidify as they cool down [31, 15];
- **BJ** (Binder Jetting), similarly to 2D inkjet printing utilizes a polymer in the form of a liquid binder, that gets deposited in droplets onto a powder bed (usually made of metallic or ceramic particles). This method can build large parts without support structures and the lack of a high power heat source cuts its cost down, but the structural properties of the final parts are poor compared to sintered equivalents, making heat treatments necessary [31];
- **Sheet Lamination**, where thin sheets of material are stacked together and bonded with adhesives or heat. This class of techniques is not entirely additive, since subtractive processes are used to cut and refine the final part, creating substantial material waste [31].

2.2.1 FDM (Fused Deposition Modeling)



FDM is a *ME* technique and the most well known *AM* process, commonly named 3D printing in popular media.

The process consists of a direct layer-by-layer deposition of a thermoplastic filament, heated up to its melting point (or enough to soften it until it reaches an optimal flow) and extruded through a nozzle [31, 15].

The nozzle is generally moved in the x-y plane until a layer is completed with the desired infill, then either the extruder head or the growth plate are moved along the z axis, initiating the printing of the subsequent layer.

The planar infill and the resolution on the z axis will determine the quality of the final print for a given material and geometry, in terms of density and visual appeal.

For a given planar infill, the z axis resolution greatly influences the final look of the part, as well as printing times: modern slicing software can analyze the geometry and generate an adaptive resolution, reducing the number of layers where the local curvature of the object is within a certain threshold and increasing it when necessary.

This approach can produce good quality parts, while reducing printing times.

FDM has gained a lot of popularity in the last few years, given its general ease of use, relatively low cost of both materials and equipment and its growing community of enthusiasts.

A wide variety of materials can be used with this technique, including (but not limited to) *PLA, ABS, PET, PETG, HIPS, TPU, nylon*.

2.2.2 SLS (Selective Laser Sintering)

SLS is a manufacturing process in the *FDF* family.

A powder bed is layed out onto a platform and a focused heat source (a laser) locally sinters the powder, until a single layer is completed [31, 15].

A mechanism wipes out the remaining powder, which is recollected and automatically redistributed by a recoating system, for each subsequent layer [5].

This process is similar to *SLM* (Selective Laser Melting), typically used with metal alloys: in *SLS* the energy input is not high enough to bring the powders to their melting point, but sufficient for sintering of the powders.

Despite the slight difference, many sources use the terms interchangeably, often effectively referring to *SLM* in metal manufacturing.

When it comes to thermoplastic materials, the required laser power to sinter each layer is substantially lower than that needed for metals.

SLS printers can be considerably more expensive than *FDM* machines of similar printing volume, but the advantages they offer, in terms of customizability, superior consistency in print quality and accuracy, higher production rate, less need for support structures, makes them a more cost effective solution for larger scale industrial production, whereas *FDM* printers are still more established in the hobbyists and enthusiasts market [5].

Generally speaking, *SLS* is a three stage process, consisting of:

- warm up (A)
- building (B)
- cooling (C)

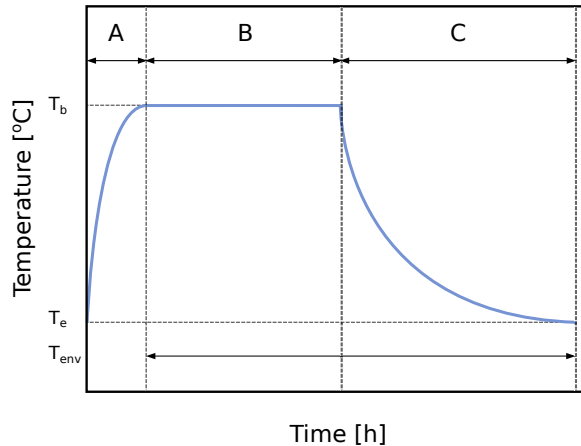


Figure 1: Phases of an *SLS* process [23, 5]



As seen in figure (1), the first phase is the time required to reach a specific powder bed temperature (T_b), based on the material of choice.

Ideally this temperature should be maintained constant inside the printing chamber, during the entire building phase, through infrared or electric heaters. The main goal is avoiding drastic temperature gradients in different areas of the printed part, since they can cause visual artefacts such as local or global deformation and, most importantly, uneven residual mechanical tension that can rapidly degrade the structural integrity of the final piece, especially in structural components that might be placed under static or dynamic loads.

Once the final piece is printed, the entire chamber is cooled down homogeneously and gradually, until the equilibrium is reached at room temperature (T_e) [5].

Quality standards for *SLS* printed parts have increased dramatically over the last few years, to the point where the manufactured components are not exclusively used for prototyping or as sacrificial items for investment casting, but they are used as finalized industrial grade parts.

However, there is still room for substantial improvements in the consistency of print accuracy, overall quality, reliability and scalability of the entire process, compared to more traditional manufacturing techniques.



The variety of physical phenomena involved in *SLS*, the fact that they can be interdependent and their different temporal regimes are the main source of complexity that makes the process inconsistent and very hard to study.

The most predominant phenomena are the following [5]:

- Laser motion and irradiation
- Thermal diffusion
- Polymer viscous flow and particle coalescence
- Powder spreading
- Solidification/crystallization



Further improvements are required in order to reduce the amount of discarded parts (still comparatively higher than most consolidated manufacturing techniques), usually defective in terms of porosity or thermal distortion or warping [5].

The next chapters will focus on potential *SLS* materials for this case study and their powder production specifically.



3 PHAs (Polyhydroxyalkanoates)

PHAs are a family of thermoplastic polyesters, obtained by hydroxyalkanoic acids via bacterial fermentation, under nutrient depletion and carbon excess conditions [15, 11].

They are a sustainable alternative to petrochemical polymers commonly utilized in additive manufacturing and they are mostly used for prototyping in the medical field [15, 11].

Similarly to other sustainable plastics, *PHA* can be produced using industrial byproducts as substrates (corn, soy, coffee, oil wastes, etc.) [15].

The monomer composition of *PHA* can be very diverse, depending on the microorganisms involved and the fermentation medium.

This variety impacts the overall mechanical, thermal and chemical properties of the final plastic, which depend on the concentration of different monomers in polymers and copolymers.

PHAs can be classified by the chain-length of their monomers [11]:

- *scl-PHA* (short-chain-length *PHA*) with 3 to 5 carbon atoms
- *mcl-PHA* (medium-chain-length *PHA*) with 6 to 14 carbon atoms
- *lcl-PHA* (long-chain-length *PHA*) with more than 14 carbon atoms

Estimating the exact meaningful measures of their properties is not always a straight-forward process, since manufacturers are not transparent about the exact composition of their products, which may have been improved by proprietary additives, whose concentration and exact composition are not usually fully disclosed [15].

The market for bioderived *PHA* has gradually increased over the years and the growth is estimated to keep its pace, given that not only are they more sustainable than competing petrochemical polymers, but they offer additional valuable properties, such as piezoelectricity and protection against gases and UV lights [15].

Their bio-origin, non-toxicity, renewability, biodegradability and biocompatibility make *PHAs* a very compelling product in the ever growing market of sustainable materials.

However, these desirable qualities contribute to their higher price, which is still not competitive against more established polymers of similar properties [15].

The increasing demand and the improvements on their biosynthesis will make their price more accessible in the future, for all sorts of applications, including additive manufacturing, where *PHAs* can be printed successfully either with FDM or SLS techniques.

3.1 PHA and Additive Manufacturing

PHAs can be used in different AM techniques, including Stereolithography, which is part of VP processes (2.2), Fused Deposition Modeling (2.2.1), where the filaments are made of a mixture of PHA and PLA, (which increases thermal stability and cuts down cost), and Selective Laser Sintering (2.2.2) [15].

This case study will focus on its usage in SLS.

PHAs have been successfully printed via SLS and utilized in the medical field as scaffolds for tissues engineering applications.

These scaffolds can be printed with a porous structure (controlled by the laser energy density), which could aid in carrying biomolecules and slowly release drugs, for instance.

Unlike with FDM applications, where PHA can not be used as a standalone filament, but needs PLA addition in order to stabilize its melting phase, PHA powders for SLS tend to maintain a better stability and their chemical composition does not get altered as easily.

This is a clear advantage, since general properties of the final products do not change drastically from its starting feedstock, and, in addition to this, the remaining powder is not thermally altered in proximity to the melt pool, meaning that it can be reused for additional printing [15].

3.1.1 PHBH

Poly(3-hydroxybutirate-*co*-3-hydroxyhexanoate) is a copolymer of the PHA family, which gained interest in the AM field and specifically in SLS applications, since it has a wider sintering window (6.1) than other polyhydroxyalkanoates such as PHB and PHBV [7, 27].

Despite having gained attention in the PHA family for SLS, especially in academic environments, the general interest for this copolymer is still relatively lower than other petrochemical polymers, due to its early-stage synthesis process, its cost and the strict confidentiality of polymer manufacturers [8].

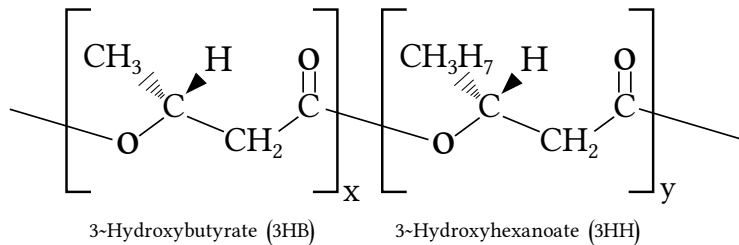


Figure 2: Schematic representation of the PHBH polymer structure [6, 23].

4 PBS (Polybutylene Succinate)

PBS is an eco-friendly biopolymer, which rose interest among industrial and academic environments. It possesses excellent properties and major benefits over comparable materials, as well as some minor drawbacks, which currently hold back its full potential.

While generally brittle, relatively expensive and still challenging to manufacture in SLS-ready powders without compromises on its environmental impact (see 6.4), this polymer has very desirable features, such as high processability (with traditional methods, at least), flexibility, as well as visual clarity and specularity. It is also thermally stable and its melting point is around 115 °C, which can make its processing, generally speaking, less energy wasting, especially when mass production is taken into account.

PBS is also easy to blend with other materials; for instance, its mechanical and thermal properties can be drastically improved when used in composite materials, where long or short fibers (or even particles) can be either randomly distributed, or woven into the polymer matrix.

Not only are fibers used for producing high tech composite materials with improved properties, but cheap natural fibers, such as palm fibers, or even blends with starches, can be utilized as an effective way to cut down cost in conventional applications, i.e. food packaging [24].

5 PBAT (Polybutylene Adipate Terephthalate)

PBAT is one of the most promising biopolymers in the sustainable plastics market, since it is very eco-friendly and, at the same time, more performant than comparable alternatives such as PHAs, which exhibit poor mechanical and thermal properties, whereas PBAT is closer to higher performance petrochemical polymers such as polyethylene terephthalate (PET) and polybutylene terephthalate (PBT) [13].

Currently used mainly in food packaging and agriculture, similarly to PBS 4, PBAT can be blended with other materials, either for technical enhancing or cost reduction.

The considerations made for PHAs and SLS 3.1 should be applicable to both PBS and PBAT, but further experiments need to be conducted and more reliable data needs to be acquired, although different studies are already showing promising results.

6 Powder production for SLS

Manufacturing raw materials for FDM is a relatively easy process, since the plastics need to be mass produced into filaments or pellets 2.2.1.

Producing powders from plastics is a much harder process.

Two radically different approaches are possible, each with its own critical issues:

- Mechanical milling
- Chemical precipitation

6.1 Powder requirements for SLS

The success rate of SLS prints is highly dependent on the characteristics of the powders involved.

The key factors in powder quality are particle size distribution, morphology, as well as thermal, flow and optical properties.

Ideally, a gaussian distribution, with most particles close to the average size is desirable, with a typical range of $(20 \div 80) \mu m$ [27].

The average particle size directly influences the layer thickness in the SLS process.

Particle morphology is crucial in the sintering mechanism, where regular, smooth and non-hollow spherical geometries are preferable [27].

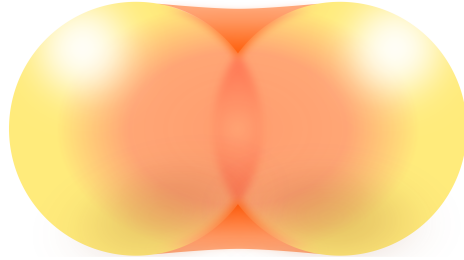


Figure 3: Two spherical powder particles forming a sintering neck [23]

The powder's density is another parameter that should be considered, as it directly correlates with the final part's global density and it allows calculation of the Hausner ratio H_r , which is a direct predictor of powder flowability.

Ideally, this coefficient should be lower than 1.4, otherwise the powder could result in issues with fluidization [27].

$$H_r = \frac{\rho_{tap}}{\rho_{bulk}} \quad (1)$$

where ρ_{tap} is the tap density and ρ_{bulk} is the bulk density of the powder.

Understanding thermal properties of the powder is essential in SLS. SLS is characterized by an optimal sintering window, with a temperature range between crystallization (T_c) and melting (T_m). For any given heat flow within that range, the material is in a metastable phase, where full coalescence of the top powder layer, as well as adhesion with previously sintered layers are most likely guaranteed [27].

Therefore, creating a tailor-made powder feedstock involves using materials with a wide enough sintering window [7, 27].

Furthermore, optical properties of the powder bed need to be taken into account, since highly reflective materials (for a given laser wavelength) can waste most of the energy input, instead of absorbing a significant amount of radiation needed to effectively melt the powder [27].

This issue is prevalent in metal SLM 2.2.2, especially with aluminum.

However, when it comes to SLS and plastics powders, the required energy is substantially lower than that needed to melt metal alloys, meaning that any potential problem with poor radiation absorbtion can be compensated by increasing the laser power output [27].

Viscosity and surface tension of the melt pool are more relevant factors when choosing powders for SLS. High viscosity and surface tension can hinder the coalescence of polymer powders and the adhesion with previously sintered layers, resulting in residual sheer stress, high porosity and thus poor quality of the 3D printed part in general.

In SLS, unlike other processes i.e. investment casting or injection molding, there is no well distributed force (e.g. built up pressure against the mold) that can increase particle coalescence and layer adhesion. The only relevant force acting on the printed part is gravity, along the vertical axis [27].

6.2 Mechanical milling

Grinding plastics into fine and homogeneous powders can be a challenge, since the high speed milling devices can easily overheat the plastics above their softening point, creating lumps of material, far from the desired result.

A solution to this problem is using so called *cryogenic grinding* devices, which utilize cooling agents such as dry ice, liquid carbon dioxide or liquid nitrogen, in order to keep the plastics below the glass transition point, where polymers become intrinsically brittle, similarly to a ceramic material, making it possible to turn the original mass into a powder [19, 17].

The heterogeneous powders can later be sieved and separated, based on their different granulometry.

Despite being an effective process for powder production, the morphology obtained with cryogenic milling is extremely irregular and unpredictable, which makes this method generally unsuitable for high quality SLS parts [27].

6.3 Chemical precipitation

There is little variety in the market of SLS ready polymer powders, with polyamide-12 (PA12) being the most optimized for this application and being produced by precipitation in ethanol [7].

Many other polymer powders can be produced using the precipitation method, but their development is currently very limited and in early-stage, especially with thermoplastics, which are not as optimized as PA12.

Most of the experimental work on the precipitation method for thermoplastics is not made available by large chemical corporations, but rather by academic environment.

6.3.1 Polymer-Solvent System

Assuming there is a potential material to use this technique with, the recommended solvent choice gravitates towards so called *moderate solvents*.

These compounds have the peculiarity of acting as a solvent only when heated above a certain temperature.

Therefore, thermoplastics can be dissolved into a compatible solvent and form a liquid-liquid phase separation upon cooling of the system, where complex crystallization and precipitation phenomena are later induced via stirring of the nucleated polymer-rich droplets [7].

A common criterion of solvent pre-selection is the evaluation of Hansen parameters, through the following equation:

$$f(\delta_x) = 100 \cdot \frac{\delta_x}{\delta_d + \delta_p + \delta_h} \quad (2)$$

which quantifies the interaction between the polymer and the solvent, in correlation with the dispersion (δ_d), the polar interactions (δ_p) and the hydrogen bond interactions (δ_h) [7].

Once the polymer-solvent system is tested, the experimental data can be effectively represented in the TEAS plot*, which helps visualizing the equation (2).

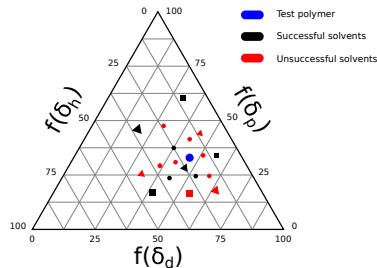


Figure 4: Generic TEAS plot for any given polymer [7, 23]

This approach has been successfully used to determine solubility of polypropylene (PP), polyethylene terephthalate (PET), polycarbonate (PC), etc, and could be effectively utilized with the target biopolymers, polybutylene succinate (PBS) (4), polybutylene adipate terephthalate (PBAT) (5) and with polyhydroxyalkanoates (PHA) such as PHBH (3).

6.3.2 Cloud point diagram

After choosing a suitable moderate solvent, the process needs to be studied and quantified with a cloud point diagram of temperature, as a function of polymer weight concentration, allowing the identification of a dissolution temperature and the temperature where LLPS (liquid-liquid phase separation) occurs. These measures allow better scalability of the process in larger controlled environments such as a reactor or autoclave system [7].

6.3.3 Production in a controlled environment

The cloud point diagram data allows for an optimization of the production process in autoclave or reactor system.

Temperature profile, initial polymer concentration and, most importantly, stirring conditions can greatly influence the final particle size distribution.

Stirring is the most impactful of these factors, producing smaller particles as the intensity increases.

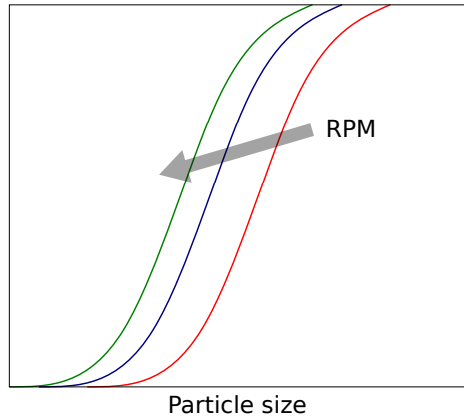


Figure 5: Particle size decreases as stirring RPM increase [7, 23]

6.4 Environmental impact

At first glance, cryogenic milling seems to be a more sustainable option for powder production. However, the issues discussed in 6.2, make this method unsuitable for SLS, unless future development will improve overall powder morphology, perhaps with the aid of post processing via thermal rounding of the

particles [7].

On the other hand, while powder production by chemical precipitation produces much better and more controllable powder feedstock, it is worth noting that organic solvents are intrinsically environmentally impactful and that should be taken into account, especially for large scale production of these powders.

The entire purpose of utilizing sustainable biopolymers in the first place might be rendered pointless, if their powder production utilizes compounds or processes that are not environmentally friendly.

Better innovative solutions (or mitigations of the mentioned issues in the current pipelines) need to be implemented in the near future.

Thermal rounding is a heat treatment, aimed at improving the bulk powder morphology for SLS applications. This kind of treatment might be the crucial step in the success of a more environmentally friendly pipeline, which does not involve any polluting solvent.

Powders can be heated either directly, with a carrier gas, or indirectly, using heated walls.

While the former method has a better process yield and reduced risk of lumping, the latter produces powders with a better, more spherical morphology, but with a significantly higher risk of particle agglomeration [1].

7 Laboratory environmental conditions and available equipment

The experimental phase of this case study has been conducted in various laboratories at *DISAT@PoliTo*.



The main production process (8) has been studied and optimized in a dedicated lab, then the residual moisture of each - cleaned and unsieved - batch of powder has been removed by oven drying (8).

Several powder samples, collected at different phases of the optimization process, have been analyzed with a *SEM* (Scanning Electron Microscope) at a third party facility (11.2), and subjected to a *TGA* (12.2) and a *DSC* (12.1) at the *Thermal Analysis* lab of the same department.

The laboratories are equipped with a large workbench and are stocked with all sorts of useful tools and equipment, especially flasks, beakers and glassware in general, as well as a chemical hood, which is essential for a safe use of chloroform (9, 9.3).

The extremely high summer temperatures and humidity were environment conditions that had to be taken into account, especially when working with chloroform, which is a highly volatile compound.

These potential issues have been addressed as later explained in detail, with adaptations and better choices among the available pieces of equipment (10, 10.2), as well as tweaking of the precipitation reaction, which in turn increased the pellet-to-powder yield by over ten-fold, compared to the initial results (9.4).

8 Choice of material and production process

 seen in previous chapters, samples of PHBH (3.1.1), PBAT (5) and PBS (4) were available for this experimental phase.

An early stage precipitation reaction had already been developed for PHBH, by other researchers at *Disat@PoliTo*. This initial recipe (9) has been tested out with the other biopolymers as well, but PHBH held the most promising results even in its early stages.

Other approaches such as cryogenic milling (6.2) have been briefly tried, but quickly discarded, due to the lack of equipment suitable for thermal rounding treatments.

The grinding procedure, aided by liquid nitrogen, proved to be successful at producing fine powders.

However, unless a thermal rounding treatment is applied, the powder morphology is too irregular and far from the ideal spherical geometry, thus making the obtained batches unsuitable for 3D printing.

All of the mentioned points led to choosing PHBH for this case study, focusing on the optimization of the available blueprint for a suitable chemical precipitation process (9, 9.3, 10).

9 Initial chemical precipitation recipe for PHBH

Researchers at *DISAT@PoliTo* started developing a prototype for a chemical precipitation reaction, derived from experiments on solute-solvent compatibility (4), which highlighted a good affinity between PHBH and chloroform.

Starting from a 4 g batch of PHBH pellets, the highest amount of sieved powder ($< 100 \mu m$) ever produced was around 1.2 g, resulting in a 30 % maximum yield.

The very early experiments were conducted using a trial and error approach, with the issues previously discussed playing a major role in the reaction's rate of success.

The environmental conditions at the time were drastically different compared to those experienced during the latest experimental activities.

Most importantly, the lab temperature was substantially lower, as the reaction was prototyped during winter.

As earlier mentioned, the extremely high summer temperatures dramatically increased the evaporation rate of chloroform, leaving a high viscosity solution that was harder to control during precipitation.

This led to failures and practically insignificant yields (9.4) if the reaction succeeded, when testing the recipe in these conditions.

After thoroughly studying the process in all its phases and isolating different variables that could have caused the issues, the recipe has been tweaked and adapted to the external conditions, which is later discussed in detail (10, 10.1).

9.1 Components

The ingredients and quantities of the prototype reaction were the following:

- 4 g of PHBH pellets
- 55 ml of chloroform
- 400 ml of 0.25 % (by weight) of PVA solution

Despite its apparent simplicity, the reaction is highly influenced by the environmental conditions, as well as equipment's correct use and proper operability.

Any slight deviation from the correct parameters, whether due to unpredictable changes in environmental conditions, malfunctioning or incorrect use of the available tools, could in fact potentially break the unstable equilibrium of the reaction, making it extremely hard to pinpoint the exact root cause of failure.

Several failed attempts, changes in equipment and tools, as well as quantities were required in order to understand the most relevant parameters of the entire process.

9.2 Equipment

All the essential pieces of equipment and tools for the reaction are listed here:

- Clean flasks and glassware for volumetric measurements, waste containment and disposal, etc
- A high precision weight scale
- A magnetic stirrer and heater
- Appropriately sized stir bars ¹
- Appropriately sized beakers for the PHBH-chloroform and the PVA solution ²
- A flow controllable dripper
- A chemical hood ³
- Distilled water for powder and tool cleaning
- A vacuum ejector
- A fritted glass filter or a paper filter ⁴
- An oven or dehydrator
- A sieve ⁵
- Sealed test tubes or any other container suitable for fine powders storage
⁶

¹A  inadequate stir bar size, in comparison to the stirring container, can be unstable and stop stirring or create undesired foams and splashes

²An adequately sized and shaped container is required for the same reason

³A chemical hood is generally required to safely operate with chemicals that produce vapours or fumes. Chloroform evaporates extremely quickly and is mildly toxic. Suddenly inhaling a large amount can cause a human to lose consciousness

⁴A porous filter combined with a vacuum ejector is preferred, as it exponentially decreases powder filtering and cleaning time

⁵A (< 100 μm) sieve was available, but smaller sizes (20 \div 80 μm) could be required

⁶Electrostatic attraction to different materials can cause significant powder losses over time

9.3 Detailed step-by-step reaction

The reaction is shortly described by the following diagram:

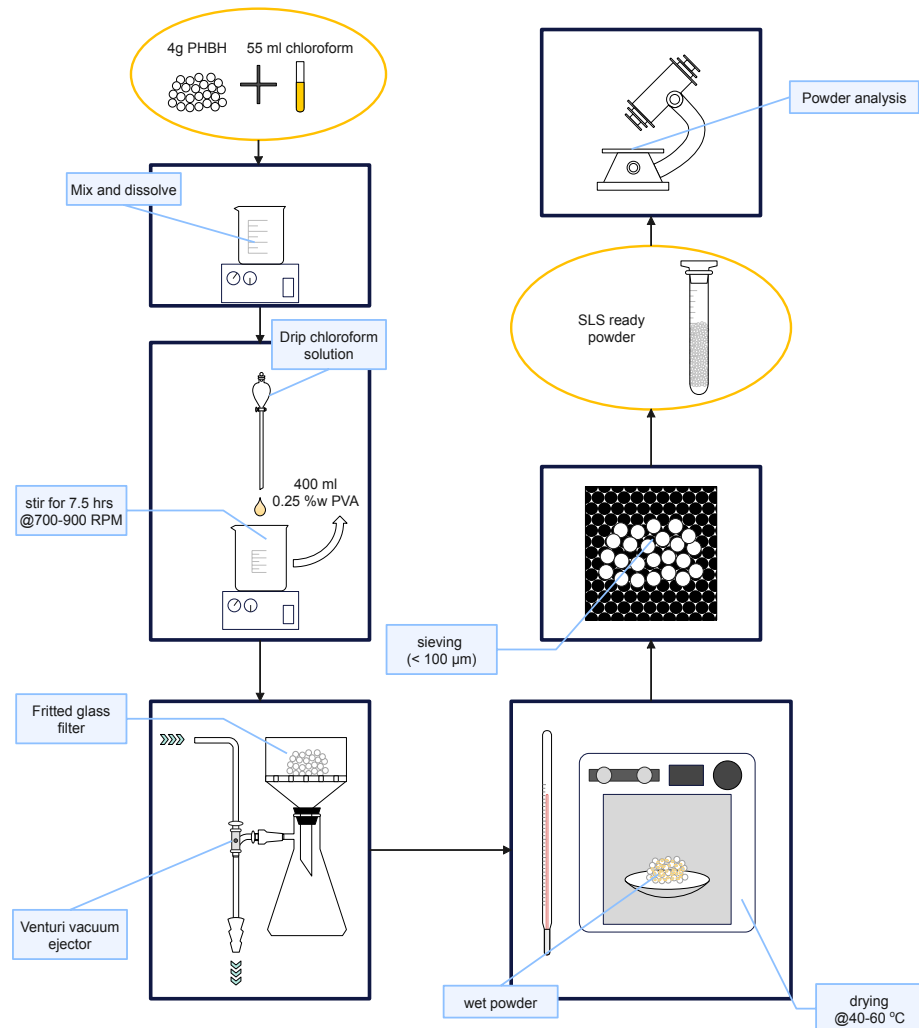


Figure 6: Process diagram [23]

PHBH pellets (4 g) need to be dissolved into 55 ml of chloroform, in order to create a viscous liquid that will later be slowly dripped into a 0.25 % PVA solution, where the precipitation occurs for a duration of 7.5 hours, at 700 rpms.

Depending on the recipient used to contain the viscous solution, the stir bar should be appropriately sized and the stirring speed should be adjusted accordingly, in order to minimize evaporation and avoid the formation of foams and splashes of chloroform.

Way too low speeds will in fact result in a long stirring time and excessive evaporation of chloroform, which leads to higher viscosity and issues with the formation of fine powders during precipitation, as previously discussed.

On the other hand, splashes and foaming can occur at excessively high stirring speeds, causing loss of liquid, or hindering the visual inspection of the solution. A visual inspection of the solution is essential, as the presence of undissolved PHBH granules or impurities can obstruct the dripper or potentially drastically reduce the final yield.

Chloroform tends to dissolve the pellets' surface extremely quickly, creating a film around each granule, that could potentially stick them together or to the container, which can lead to a significant delay in total dissolution time.

It is best practice to slowly drop PHBH pellets into chloroform while already being stirred, instead of pouring the solvent onto the granules, in order to avoid the aforementioned issues.

Once the solution is ready, it can be poured into the flow controlled dripper. The flow rate can be controlled through a manual valve and should be adjusted periodically, as the column of fluid diminishes in height with time, reducing the total weight that pushes more fluid down the thin channel. The solution can dry and create a plastic film all around the dripper's walls, reducing the cross section of the last thin trait over time. Flow rate should be manually adjusted to compensate this issue as well.



Ideally, the chloroform solution should flow in a fast paced but drop-by-drop fashion.

The flux valve can be extremely sensitive and hard to control manually, so occasional large bursts of fluid can suddenly end up in the PVA solution. However, as long as this phenomenon does not occur too frequently and is dealt with in a timely manner by closing the valve and slowly readjusting the flow, it does not seem to affect the precipitation process in a significant way (10.1).

The 400 ml of 0.25 % PVA solution should be ready in advance and already set at the proper stirring speed, before the dripping process begins.

The percentage of PVA is extremely low and it is best practice to prepare a higher concentration solution, in large batches, that can be further diluted and

utilized when needed.

Batches of 1 kg PVA solution (1 % by weight) were prepared and stored in a refrigerator.



Figure 7: A bulk preparation of PVA solution.

The initial approach was utilizing mass units only, however PVA can be hard to dissolve in water at room temperature.

Different batches were prepared by gradually increasing the operational temperature, regulated by a magnetic stirrer-heater.

Unless water temperature was kept substantially high (above 70 °C but still lower than boiling point), solid PVA flakes remained undissolved, despite being stirred for hours.

Regardless, defective batches were used during the early experiments, but the undissolved PVA seemed to create a slimy solution that, over time, would produce a thick foam, that potentially clogged the fritted glass filters.

Temperatures have been kept higher since then, resulting in no filtering issues down the pipeline.

However, despite being able to fully dissolve the solute, water evaporated consistently, making it necessary to refill the container with distilled water, until 1 l of total solution was reached.

This was clearly an approximation, compared to the initial choice of utilizing mass measurements only, however the error of a volume filling approach can be considered negligible, given that the percentage of PVA is only 1 % by weight and the solution needs to be further diluted down to 0.25 % for the precipitation reaction.

Dilution to the required fraction of mass is simply obtained by using 100 ml of 1 % solution, plus 300 ml of water, for a total of 400 ml.

The precipitation reaction is left stirring for 7.5 hours under a chemical hood, starting from the very first drop of PHBH-chloroform solution.

This time frame is extremely conservative, as it is very likely that all the residual chloroform is entirely evaporated in a much shorter time, however this aspect has not been tested yet.

At the end of the waiting time, the solution can be filtered with a fritted glass filter, aided by a vacuum ejector.

After the PVA solution is filtered out, the remaining powder bed should be washed with isopropyl alcohol and distilled water.

Paper filters can be utilized, but the filtering phase would last exponentially longer. Furthermore, the vacuum filtering approach can get rid of almost all of the residual moisture.

The obtained powder bed needs to be dried in an oven or a dehydrator, at 40 °C, for at least 12 hours.

At this point, the powder should be completely dry and ready to be sieved.

A 100 μm sieve has been used, however, smaller size sieves could be used, as many reviews recommend a particle size of 20 \div 80 μm for SLS 2.2.2.

Powders should be gently pushed against the mesh, alternating with circular motion and shaking of the sieve, should an automated sieving system be unavailable.

Several passages might be needed in order to collect most of the powder.

Sieved powders should be immediately stored in test tubes or any other sealable container, as they are extremely hygroscopic.

With very fine powders, electrostatic interactions with tools and materials should be taken into account, when transferring them into containers.

Some losses are expected during this phase, unless specific tools for collecting very fine powders are available.

Choosing appropriate materials and reducing material transfer to the minimum amount is essential to minimize powder losses.

All tools and containers should be perfectly dry too.

9.4 Initial results and failures

As mentioned in previous chapters, many failed attempts led to a deeper understanding of the entire process and the proper choice of equipment, tools and tweaking of the initial recipe.

The most prominent issue were the environmental variables. With temperatures constantly exceeding 30 °C, the 55 ml of chloroform, initially used by previous researchers during winter, evaporated too quickly while PHBH pellets were being dissolved.

The obtained liquid was extremely viscous and hard to drip effectively into the PVA solution. Drippers were constantly clogged and flow control via manual valves was unpredictable, to say the least.

A thick plastic film covered the internal walls of the drippers and the beakers where PHBH had been dissolved, which introduced the very first significant material waste point in the pipeline.

Moreover, despite being impossible to avoid in general, the excessive thickness of this film that formed in the first batches severely hindered the cleaning and maintenance of the utilized glassware, which occasionally needed to be cleaned with chloroform or other solvents.

Despite being able to save most initial batches, the final yield was insignificant, going as low as 0.1 g of powder per 4 g of raw material.

Another factor that severely reduced production rate was the frequent clogging of fritted glass filters.

The undissolved PVA flakes in the first defective batches (9.3) created a dense foam, which either obstructed the pores of the filter or slowed the filtration time by orders of magnitude.

The clogged filters required to be regenerated with chloroform and rinsed with isopropyl alcohol, in order to regain full functionality.

In addition to this, some of the filters initially used had already been exploited by other research teams, operating with metal fines and other materials, which might have contributed to some of the impurities and alien particles detected by SEM analysis in the earliest samples (11.2).

10 Recipe tweaking and improvements

All of the aforementioned failed attempts (9.4) led to an optimization process that originally aimed at matching the 30 % yield (9) obtained by previous researchers (who provided the prototype recipe but worked in different environmental conditions), but later far exceeded the initial expectations, improving upon the available blueprint procedure by a wide margin.

10.1 Key variables

Dealing with a simple yet unstable process, based on theoretical studies and very rough experimental data, requires a long trial and error approach, that should carefully isolate each variable, whether it is intrinsic to the involved physical and chemical reactions, environmental, equipment related, or introduced by human interaction with the process.

Generally speaking, once all the independent variables are isolated and understood, only a few are extremely relevant and can radically influence the success rate of the entire process.

Should these variables be changed, even unintentionally and by a small amount, the final yield could be dramatically cut down.

It has been pointed out several times that the external temperature is one of the most (if not the absolute most) influential parameter of the entire process, given the fast evaporation pace of chloroform, or organic solvents in general, should the reaction be re-engineered with a less impactful solvent, like the moderate solvents often mentioned in the scientific literature (6.3).

For all the issues discussed in previous chapters, an increase in external temperature correlates with an increase in chloroform use. Starting from the initial 55 ml per 4 g of PHBH pellets, extra chloroform has been added by 2.5 ml increments, until the process stabilized and yield reached a peak that would not benefit from further increase.

The maximum useful amount of chloroform (per 4 g of PHBH pellets) would be around $65 \div 70\text{ ml}$.

This range consistently produced the highest yield (10.3) and not only did further chloroform use stall the results, but it proved to be detrimental over a certain threshold ($> 75\text{ ml}$), as insufficient viscosity would prevent an accurate flow control during the dripping phase.

All these adjustments in chloroform quantity are only a consequence of uncontrolled operational temperatures. A 10 ml increase in chloroform use might seem insignificant at a lab scale, but this would translate to significant waste, should the process be scaled to an industrial level (10.4).

This consideration ties with the environmental sustainability issue (6.4), since organic solvents are inherently impactful and unnecessary waste should not be promoted, especially when sustainable biopolymers such as PHBH are involved.

Overall, the key parameter that actually matters is viscosity: very low temperatures can minimize chloroform evaporation, but directly increase density and thus viscosity; on the other hand, liquids at higher temperatures should be inherently less viscous, but the drastic solvent evaporation dramatically increases viscosity, simply by having more PHBH and less liquid proportionally.

The process should be tailored to obtain a PHBH-chlofororm solution with the ideal viscosity, that allows a perfect dripping phase, while producing the highest pellet-to-powder yield.

However, future experiments should focus on achieving this goal with the lowest amount of chloroform possible, which requires being able to control operational temperature.

By contrast, other variables like dripping flow (as previously discussed a drop by drop fashion is ideal but occasional flow disruptions do not seem to have a great influence (9.3)), or a very precise measure in PVA concentration are not as important for the success of the precipitation process.

With a PVA concentration as low as 0.25 % and successful reactions even with defective solution batches, it is plausible that the precipitation process could be accomplished by substituting PVA with other alcohols such as isopropanol or ethanol or even by simply using distilled water ⁷.

Assuming the adjustment of viscosity and the optimization of the dripping phase have been dealt with, another relevant parameter is the stirring speed of the PVA solution (9.3).

The experiments conducted during this case study confirm what has been found in the scientific literature: an increase in stirring speed directly correlates to a decrease in average powder particle size (5).

However, this correlation is generally measured in terms of RPM, which is an active control of any magnetic stirrer and a good indication of the average rotational speed of the stirred fluid, assuming that the device is properly functioning and every other variable is fixed.

In fact, the RPM controlled by the machine does correlate with the average angular velocity, but does not indicate an exact speed value.

For any fixed fluids, should other factors like container size and shape, stirring rod weight and size change, then the average angular velocity would change as well, despite the stirrer being at a fixed RPM value.

Since the production rate had been doubled to 8 g of pellets per batch, the reaction has been split into two 4 g batches, for lack of single batch capable equipment.

Despite perfectly measuring all the quantities and mirroring equipment use for both batches, the magnetic stirrers' reported RPM did not match the uneven velocities (even though the utilized models were exactly the same).

⁷These substitutions would immensely simplify the production of the precipitation solution for the previously discussed issues of dissolving PVA (9.3), but no experiments have been conducted yet

This aspect is later discussed in further detail ([10.2](#)).

Once this issue has been partially solved with some workarounds, increasing RPM has proven to be an effective strategy to increase final yield: powders were effectively produced at the initially planned 700 RPM, however most of the powder batch could not be sieved under $100\ \mu m$.

Higher RPM values produced almost no waste during the sieving phase.

10.2 Adaptations and progressively refined equipment choice

Some of the available equipment was not perfectly suited for the necessary tasks or, sometimes, even broken or malfunctioning.

For instance, the drippers used for the precipitation reaction had a manual flux valve, which made flow control unpredictable and hard to regulate.

The fritted filters initially used had already been utilized for other production pipelines, transferring some impurities to the first samples. This issue was addressed by utilizing a new batch of filters, solely dedicated to the PHBH pipeline.

A major issue was the malfunctioning of one of the magnetic stirrers. This caused a few batches to be lost, since the prolonged absence of a stirring motion did not allow for the precipitation process to occur.

The defective stirrer was replaced, however, a huge discrepancy in stirring speeds was noticeable, as briefly mentioned in the previous chapter ([10.1](#)).

In spite of the fact that both solutions were prepared identically and the beakers and stirring rods used were exactly the same, one of the stirrers would visibly show a much lower speed at the same RPM value.

As an initial workaround, a satisfying speed (based on previous results in terms of final yield) was set on the slower stirrer, then the much faster stirrer was set at a "lower" RPM value, that would visually match the same angular velocity as the reference.

This issue was addressed by utilizing two identical stirrers from the same manufacturer, which were set at the same RPM value.

Adaptations were needed for storing the sieved powders. With average particle sizes under $100\ \mu m$, electrostatic interaction and powder volatility proved to be challenging when handling the final product.

Sieved powders have been transferred to test tubes or other comparable containers by using folded parchment paper.

All the workarounds and adaptations can normally be part of a very experimental lab workflow, but the process should ideally be capable of producing even greater yields, once it is scaled for industrial production, where each step is standardized and custom equipment tailored to specific tasks.

10.3 Current results

Compared to the earliest batches, even the experiments conducted by previous researchers held substantially better results, with maximum yields of 30 %.

The minimum requirement for the current case study was that of replicating the previous records but, after a huge amount of failed attempts, optimization and tweaking in the entire process pipeline, current results far exceed the initial expectations, with even more room for improvement.

The pellet-to-powder yield has increased to a minimum of 5 g of powder and a maximum of 6 g, over 8 g of raw material.

The current yield ranges between 62.5 % and 75 %, which is a relative improvement of 2 ÷ 2.5 times that achieved in the previous research that this work is based on, and over an order of magnitude increase compared to the initial experiments.

10.4 Consistent reproducibility and scalability

Not only has the total yield been improved, but the process has been stabilized and better understood in all of its peculiarities ([10.1](#)).

Until all the optimization work had been accomplished, the process held inconsistent results, with powder quantities drastically varying from insignificant to mediocre yields.

A key aspect of a reliable process is in fact its consistent reproducibility under known and controllable conditions, which is necessary (but not sufficient) for large scale production and adoption at industrial scale.

The latest results have been reproduced consistently in the lab and might be scaled to higher production rates after further optimization.

11 Powder granulometry and morphology

While obtaining some form of powder with the precipitation process was somewhat expected, all the work would be pointless if the criteria discussed at the beginning of this research (6.1) were not met.

The powders produced would not be suitable for SLS additive manufacturing, if granulometry (average grain size distribution) were not under a certain size threshold and if the morphology of those powders were not close to a non hollow spherical geometry [5].

While proper granulometry is guaranteed by sieving the powders (11.1), as later confirmed by particle size distribution investigations (15), adequate morphology can only be determined by thoroughly inspecting SEM images (11.2).

11.1 Sieving process

Sieving is an essential step when selecting SLS suitable powders.

A general guideline on SLS powders granulometry is that particles should be smaller than $100 \mu m$, with many sources in the literature reporting an ideal range of $20 \div 80 \mu m$ (11).

The powders obtained during the first experiments produced a lot of waste during the sieving phase, where a $100 \mu m$ sieve has been used to collect suitable samples.

With the current optimized process, the powder batches are almost entirely sieved, producing little to no waste during this phase.

11.2 SEM (Scanning Electron Microscope) analysis

Scanning Electron Microscopes are widely used detection instruments, which unlike traditional microscopes do not utilize optical lenses, but reconstruct images generated by the interaction between an electron beam and the targeted sample.

There are several inspection techniques that could be exploited using different SEMs, however the most suitable for inspecting fine powder morphology is the image reconstruction through SE (Secondary Electrons) emission.

When invested by a high energy electron beam, the inelastic interaction with secondary low energy electrons ($< 50 \text{ eV}$) triggers their emission from the valence bands of the specimen atoms and scatters them.

The emission of secondary electrons happens within a few nm inside the specimen, which makes this method perfectly suited for highlighting particle overall shape and surface displacement, to a high degree of detail and precision.

SEM images have been produced with multiple specimens, on samples collected during the entire duration of the experimental activities, which is later discussed in detail ([11.2.1](#)).

The expected particle morphology should ideally approach that of perfect non hollow sphere, as pictured below.

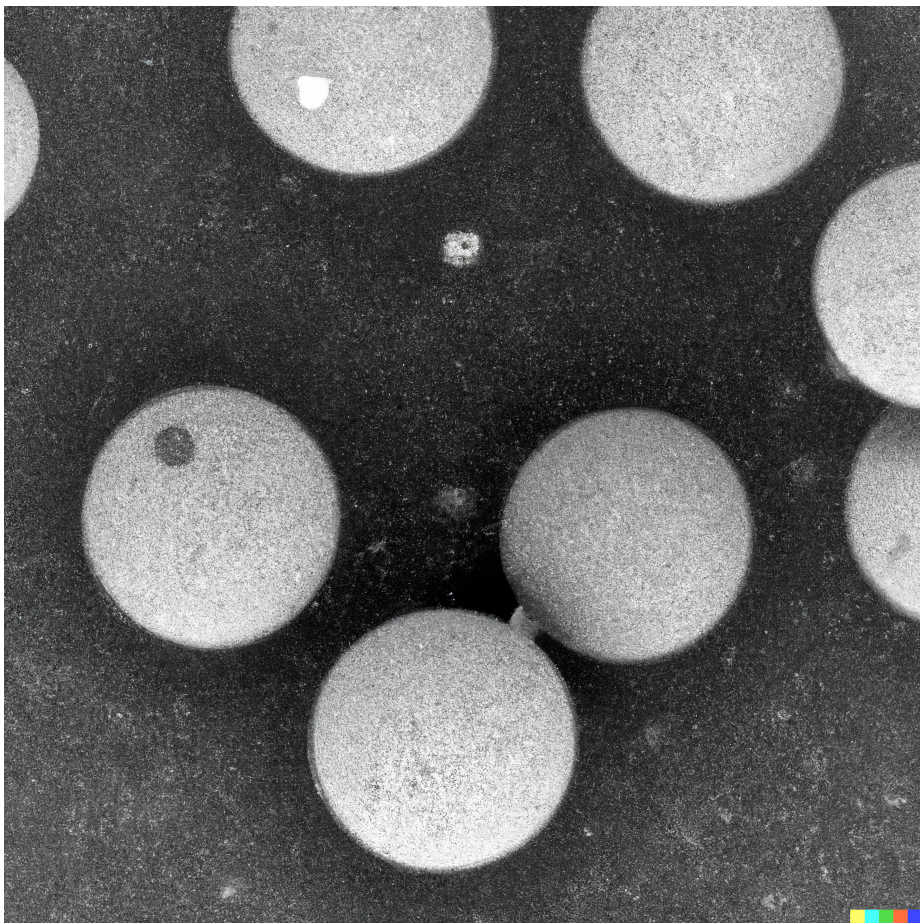


Figure 8: "Round particles seen through a SEM microscope" as imagined by Dall-E 2's artificial intelligence algohorithm [2, 3]

11.2.1 Results

As mentioned, samples have been collected throughout the entirety of the experimental activity, which has been characterized by a lot of trial and error, before the entire production pipeline got optimized and under perfect control (10).

The experiment has been conducted using a *FIB-SEM, TESCAN S9000G, Tescan* instrument, which is a high resolution scanning electron microscope, equipped with a focused ion beam (FIB) for sample preparation and an electron backscatter diffraction (EBSD) detector [29].

The collected specimens have been selected, categorized and then assigned an ID:

$$ID = SEM_{NN} - nnnX_{(SignalA)} \quad (3)$$

where SEM_{NN} is the sample's absolute ascending time number, $nnnX$ is the magnification factor and $(SignalA)$ is the signal type used by the instrument to generate the image.

All the selected samples have been catalogued as follows:

ID	EHT [kV]	WD [mm]	Magnification	Signal A	Date [dd/mm/yyyy]	Time [hh:mm:ss]
$SEM_01 - 461X_{(SE1)}$	10.00	8.65	461 X	SE1	12/07/2022	15:21:07
$SEM_02 - 461X_{(SE1)}$	10.00	8.60	461 X	SE1	12/07/2022	15:22:19
$SEM_03 - 461X_{(SE1)}$	10.00	8.60	461 X	SE1	12/07/2022	15:22:41
$SEM_04 - 461X_{(SE1)}$	10.00	8.60	461 X	SE1	12/07/2022	15:24:52
$SEM_05 - 461X_{(SE1)}$	10.00	8.60	461 X	SE1	12/07/2022	15:25:31
$SEM_06 - 461X_{(SE1)}$	10.00	8.60	461 X	SE1	12/07/2022	15:27:17
$SEM_07 - 800X_{(VPSE G4)}$	20.00	8.64	800 X	VPSE G4	03/10/2022	18:46:15
$SEM_08 - 800X_{(VPSE G4)}$	20.00	8.64	800 X	VPSE G4	03/10/2022	18:49:02
$SEM_09 - 800X_{(VPSE G4)}$	20.00	8.76	800 X	VPSE G4	03/10/2022	18:51:15
$SEM_{10} - 400X_{(VPSE G4)}$	20.00	8.76	400 X	VPSE G4	03/10/2022	18:54:00
$SEM_{11} - 400X_{(VPSE G4)}$	20.00	8.76	400 X	VPSE G4	03/10/2022	18:55:21
$SEM_{12} - 400X_{(VPSE G4)}$	20.00	8.76	400 X	VPSE G4	03/10/2022	18:56:40

Table 1: All catalogued SEM samples

The samples have been collected in a total of 12 different occasions, with a total of 12 different specimens.

The main instrument parameters to be modified during the experiment were the electron beam energy, the working distance, the magnification factor and the signal type.

The electron beam energy has been set to 10 kV for the first 6 samples, using the secondary electrons signal at constant pressure (SE) and then to 20 kV for the remaining 6 samples, using the variable pressure secondary electrons signal (VPSE G4).

Different magnifications factors have been used, ranging from 400 to 800 X, to showcase different particle sizes and to better understand the particle morphology.

All SEM images have been AI upscaled and enhanced with basic raster image editing workflows.

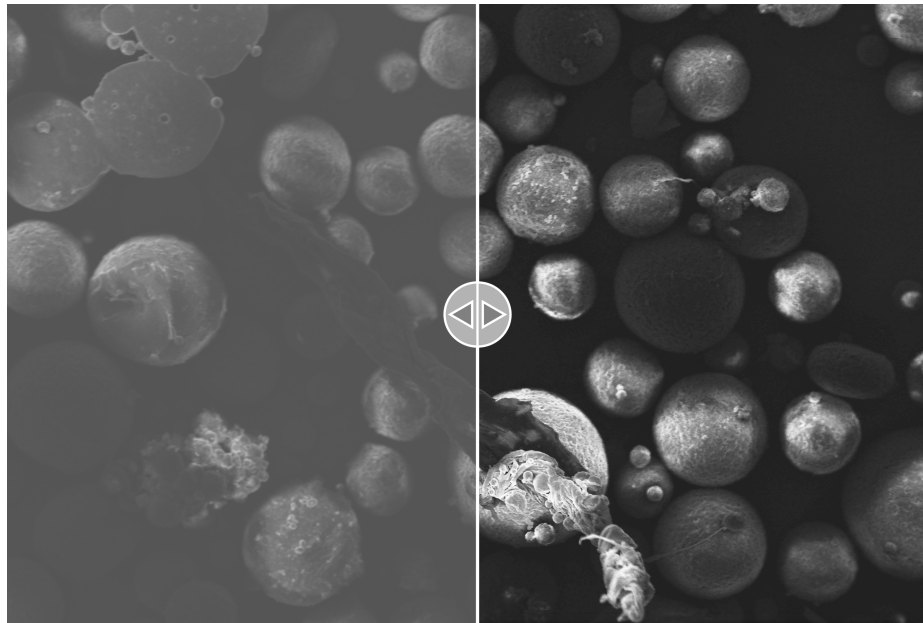


Figure 9: Example of a SEM image before and after [enhancing](#) [23, 28]

The FIB-SEM instrument has produced a total of 12 different images, which are shown below:

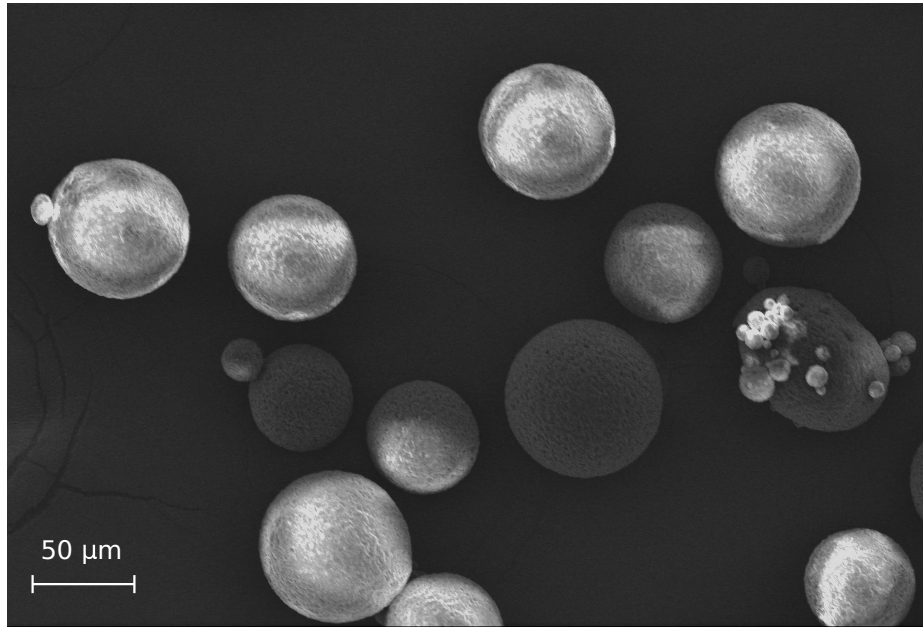


Figure 10: Enhanced SEM image, $SEM_{01} - 461X_{(SE1)}$ [28, 21]

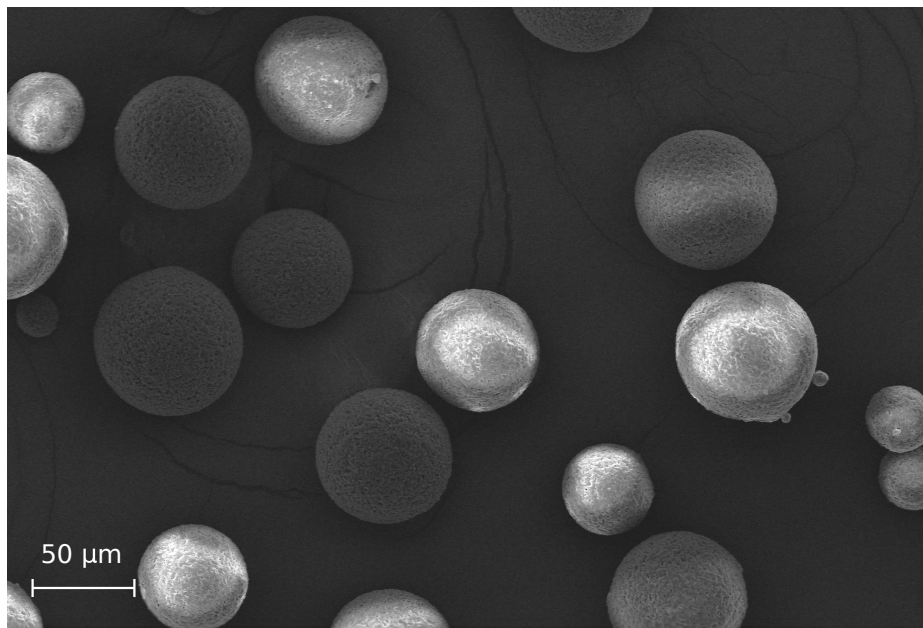


Figure 11: Enhanced SEM image, $SEM_{02} - 461X_{(SE1)}$ [28, 21]

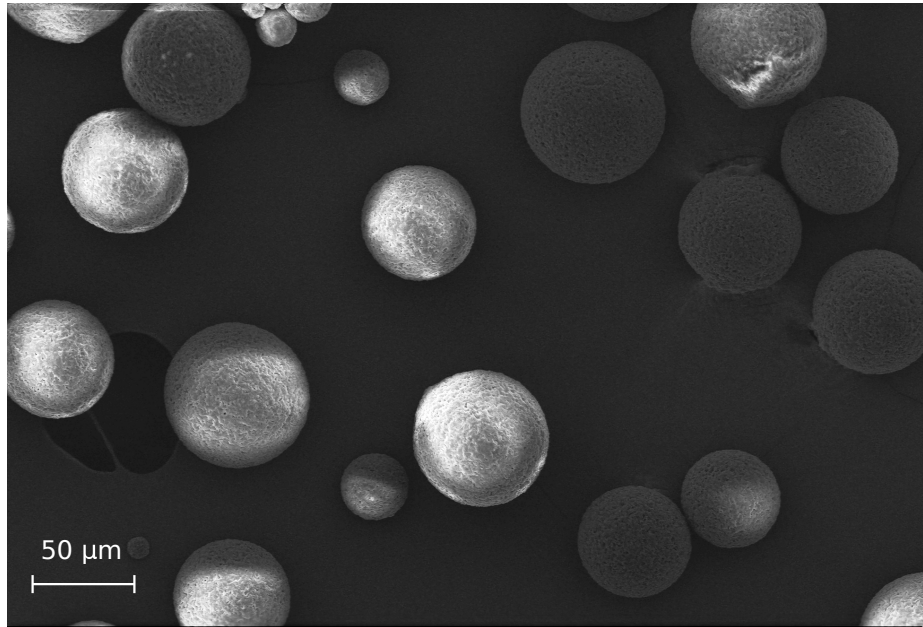


Figure 12: Enhanced SEM image, $SEM_{03} - 461X_{(SE1)}$ [28, 21]

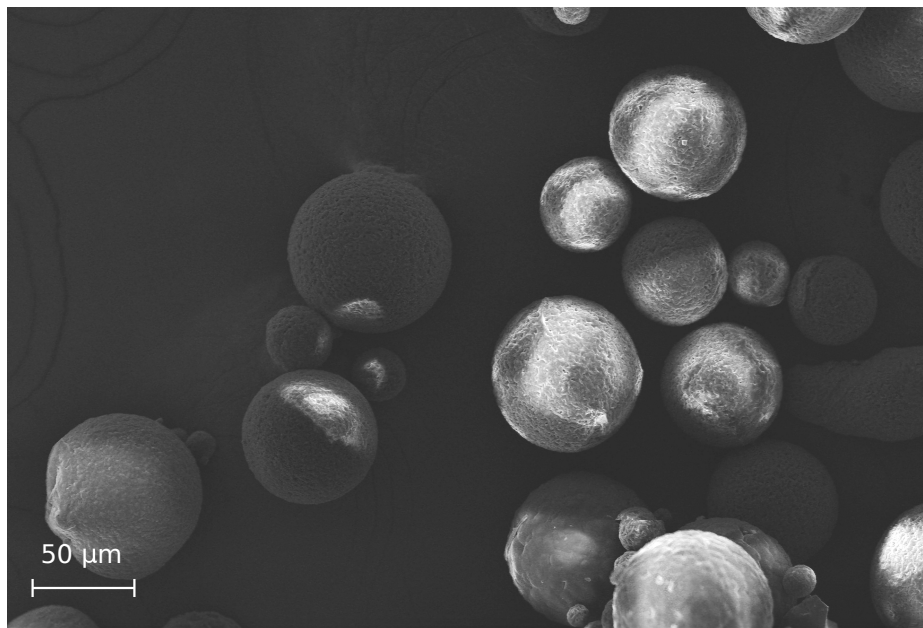


Figure 13: Enhanced SEM image, $SEM_{04} - 461X_{(SE1)}$ [28, 21]

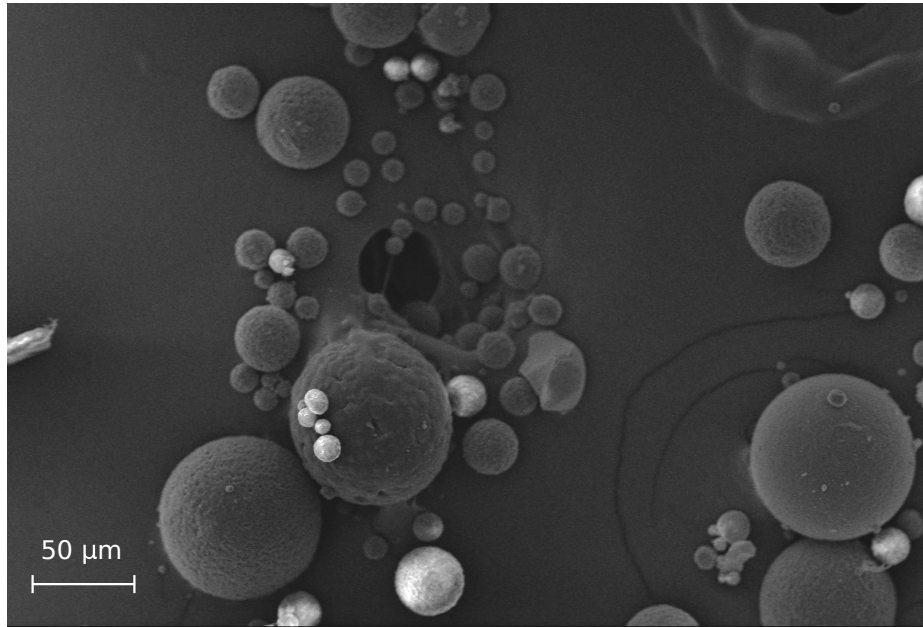


Figure 14: Enhanced SEM image, $SEM_{05} - 461X_{(SE1)}$ [28, 21]

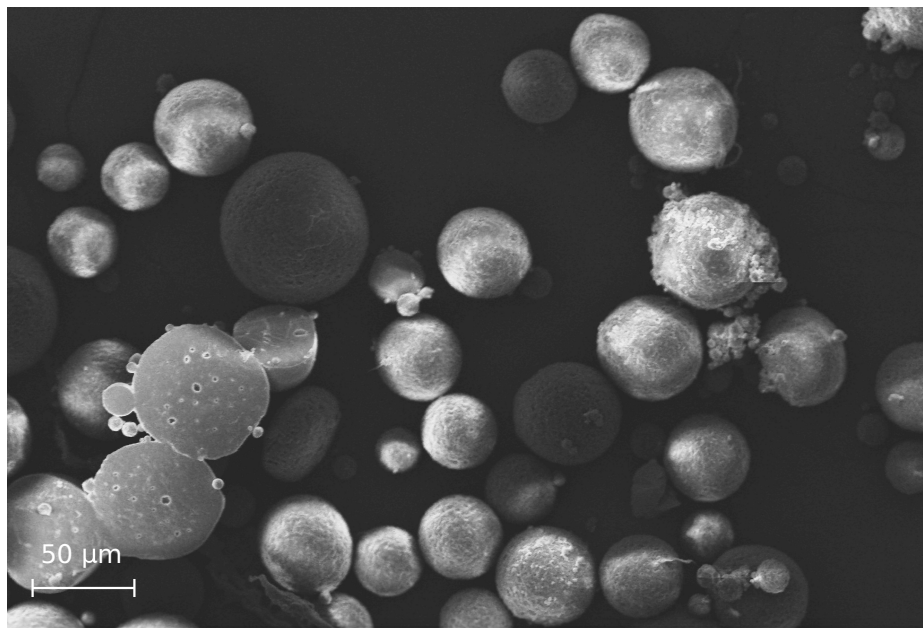


Figure 15: Enhanced SEM image, $SEM_{06} - 461X_{(SE1)}$ [28, 21]

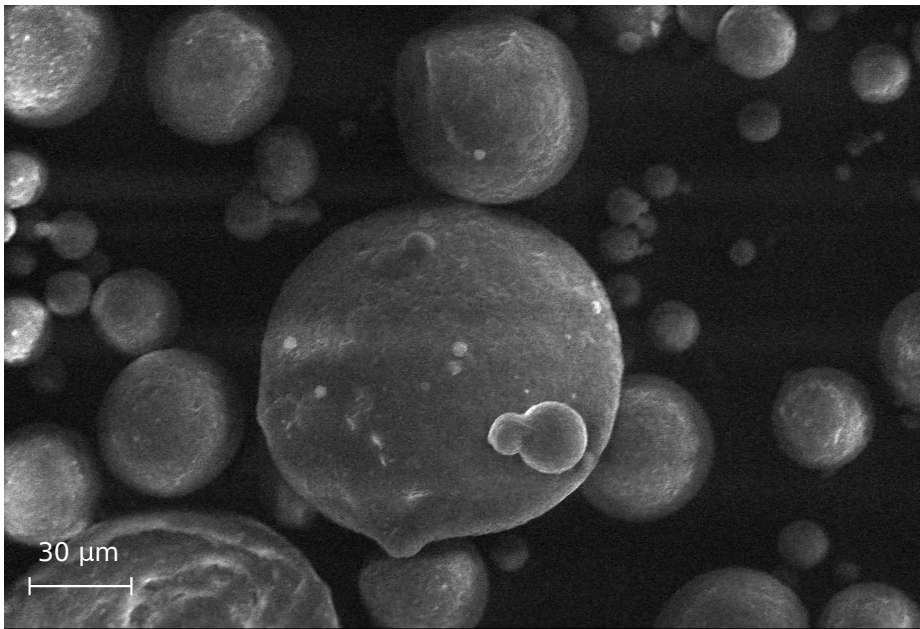


Figure 16: Enhanced SEM image, $SEM_{07} - 800X_{(VPSE\ G4)}$ [28, 21]

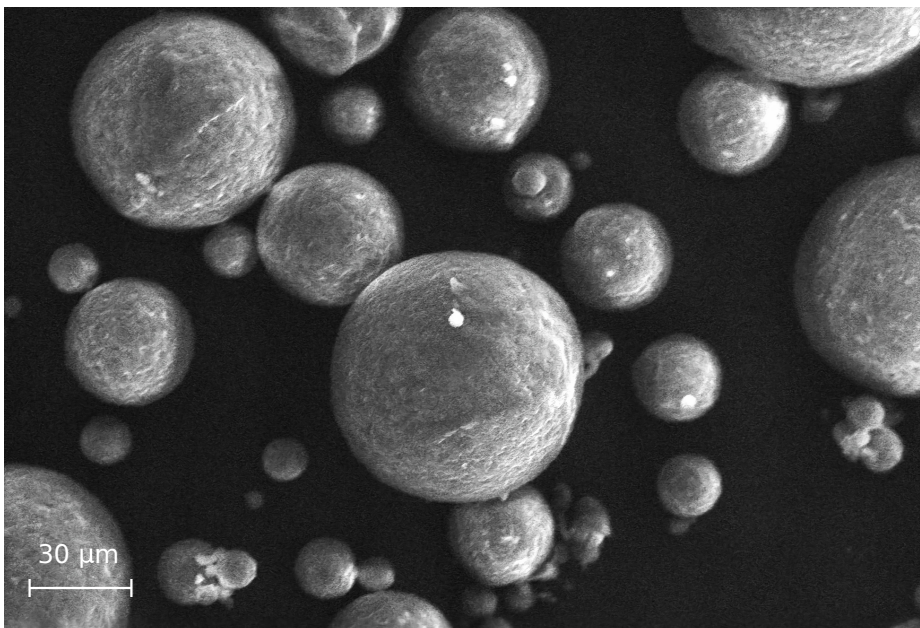


Figure 17: Enhanced SEM image, $SEM_{08} - 800X_{(VPSE\ G4)}$ [28, 21]

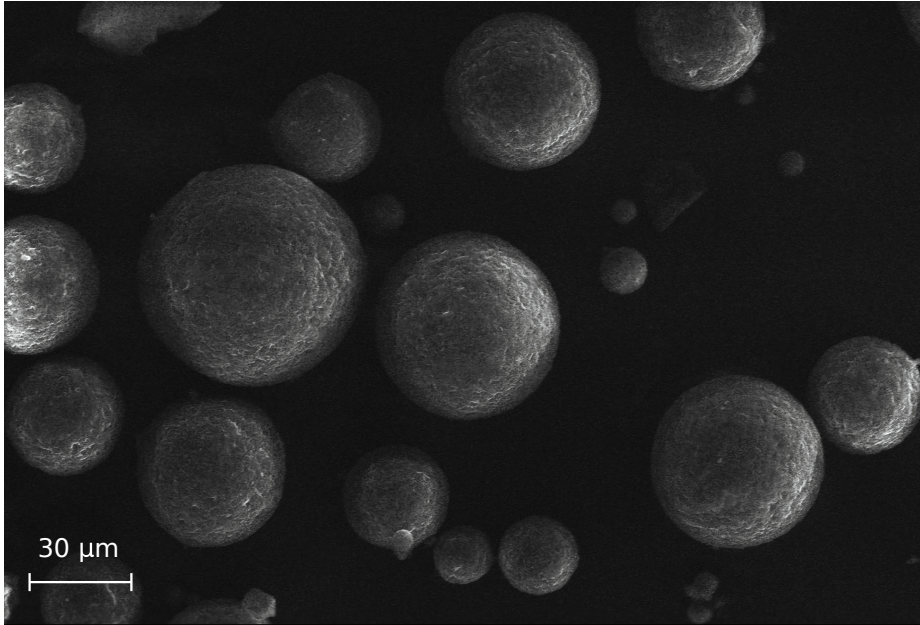


Figure 18: Enhanced SEM image, $SEM_{09} - 800X_{(VPSE\ G4)}$ [28, 21]

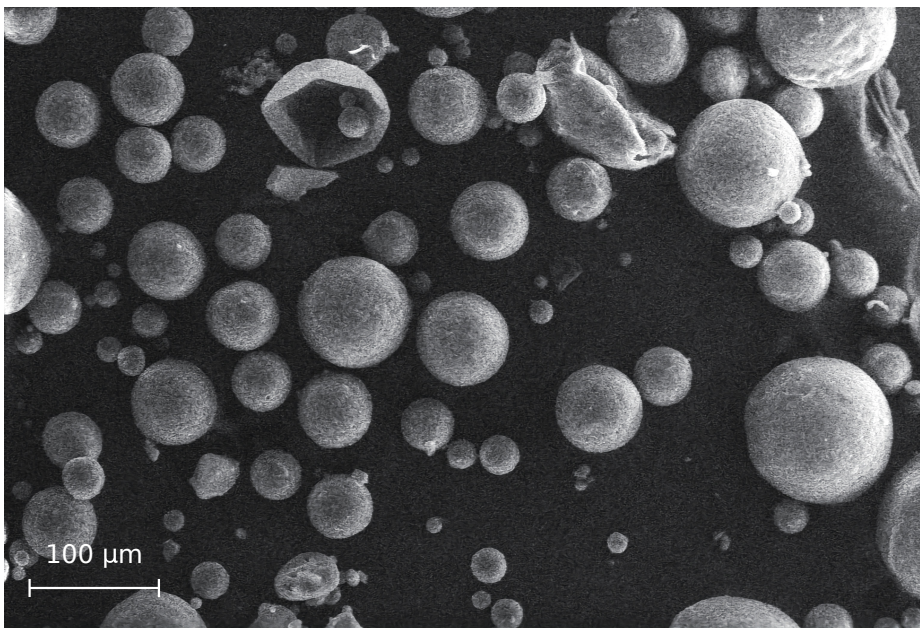


Figure 19: Enhanced SEM image, $SEM_{10} - 400X_{(VPSE\ G4)}$ [28, 21]

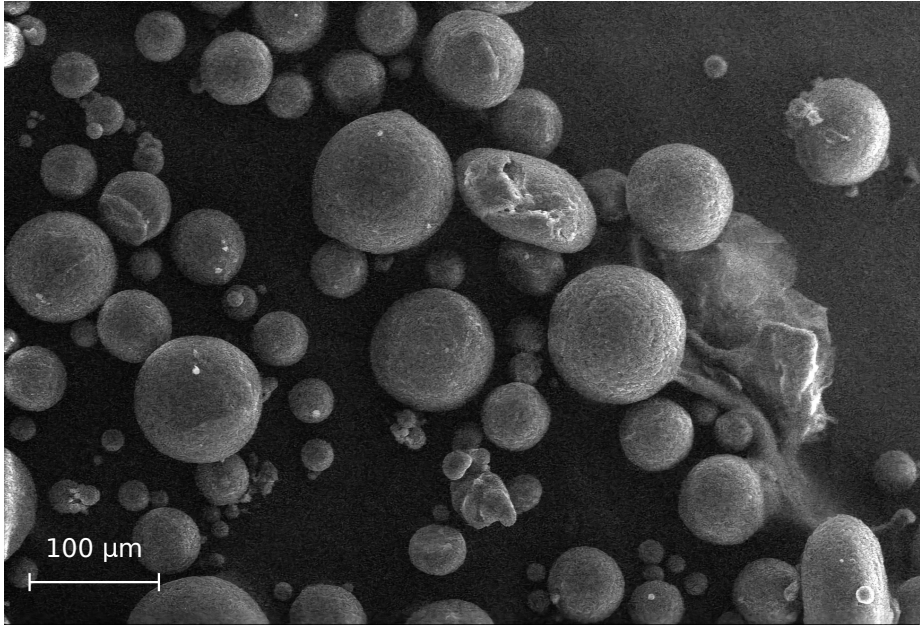


Figure 20: Enhanced SEM image, $SEM_{11} - 400X_{(VPSE\ G4)}$ [28, 21]

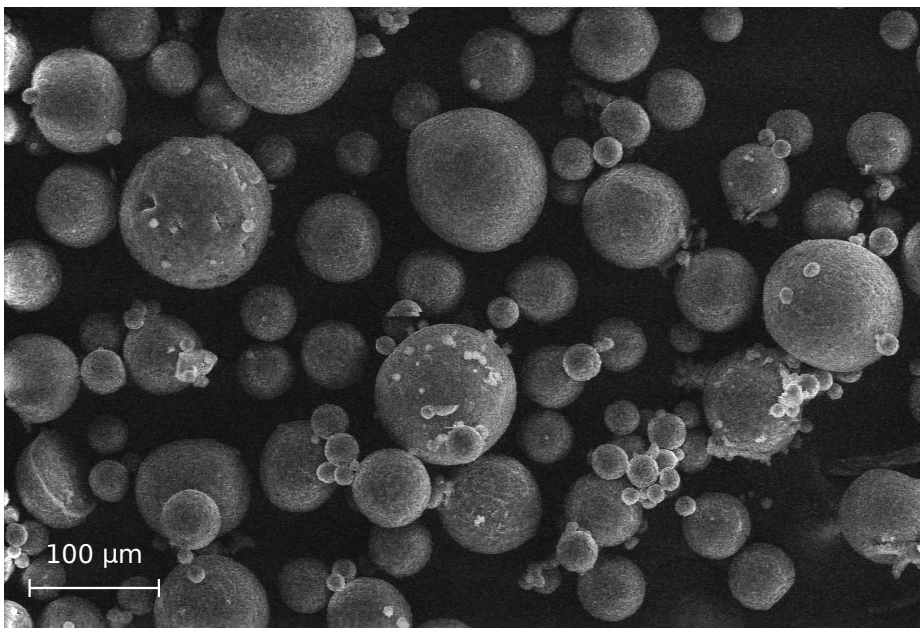


Figure 21: Enhanced SEM image, $SEM_{12} - 400X_{(VPSE\ G4)}$ [28, 21]

12 Thermal analysis

Thermal analysis tools have been utilized in this case study, as many critical properties of the studied material can be deducted with different measurements at various temperature ranges.

This is especially true with materials suited for SLS, where knowledge of thermal properties is essential in determining a polymer's feasibility for this AM method. The thermal analysis tools used in this case study are the Differential Scanning Calorimetry (DSC) and the Thermogravimetric Analysis (TGA).

12.1 DSC (Differential Scanning Calorimetry)

Differential Scanning Calorimetry is a thermoanalytical technique that can be implemented with different types of machines, but its general purpose is the analysis of the change in heat flux as a function of temperature, which is generally increased in a linear fashion.

The term differential in DSC indicates that each test sample is analyzed in parallel to a reference sample, whose heat capacity and thermal properties are well known and used to calibrate the machine.

A typical use of DSC is the detection of phase transitions, which is crucial for applications such as SLS, where each material needs to be locally fused within an optimal sintering window (6.1, 3.1.1).

One of the greatest advantage of PHBH over comparable materials is its wider sintering window, which makes it ideal for SLS (3.1.1).

This sintering window can be measured by analyzing a DSC plot of heat flux over temperature, given that this test measures phase transitions but is also capable of detecting more subtle physical changes, such as glass transition. Since the sintering window is defined as the temperature range comprised between cold crystallization offset and melting point onset (6.1), both detected by a DSC analysis (23), then calculating it is trivial, based on the available data.

12.1.1 Results

The DSC machine used in this case study is the *Mettler-Toledo DSC-1 STARe System*, which is a benchtop instrument that can be used for a wide range of applications.

It is equipped with a *Gas Controller GC100*, in the temperature range from $-50\text{ }^{\circ}\text{C}$ to $180\text{ }^{\circ}\text{C}$ with a heating rate of 10 (or 5) C/min , and from 180 to $-50\text{ }^{\circ}\text{C}$ with a cooling rate of $10\text{ }^{\circ}\text{C}/\text{min}$, under nitrogen flow ($50\text{ mL}/\text{min}$).

The included *Mettler-Toledo STARe software* (V12.10) allows for the analysis of the DSC data, as well as the creation of a report with the results.



Figure 22: Mettler-Toledo DSC-1 STARe System [30]

Multiple DSC analysis have been conducted and specimens have been catalogued with the following ID:

$$ID = xDSC_{(n^\circ C/min)} - NN \quad (4)$$

where x is either P for pellet or p for powder, n is the temperature range, and NN is the sample's absolute ascending time number.

The specimens have been catalogued as follows:

ID	Weight [mg]	Temperature ramp [$^{\circ}\text{C}/\text{min}$]	Type
$PDSC_{(10 \text{ } ^{\circ}\text{C}/\text{min})} - 01$	8.5000	10	pellet
$pDSC_{(10 \text{ } ^{\circ}\text{C}/\text{min})} - 02$	8.0000	10	powder

Table 2: DSC specimens

The analysis results have been analyzed and plotted using *Labplot* [14] and *Inkscape* [23], using the *exo-up* convention, with the raw pellet curves used as a baseline for the powder curves.

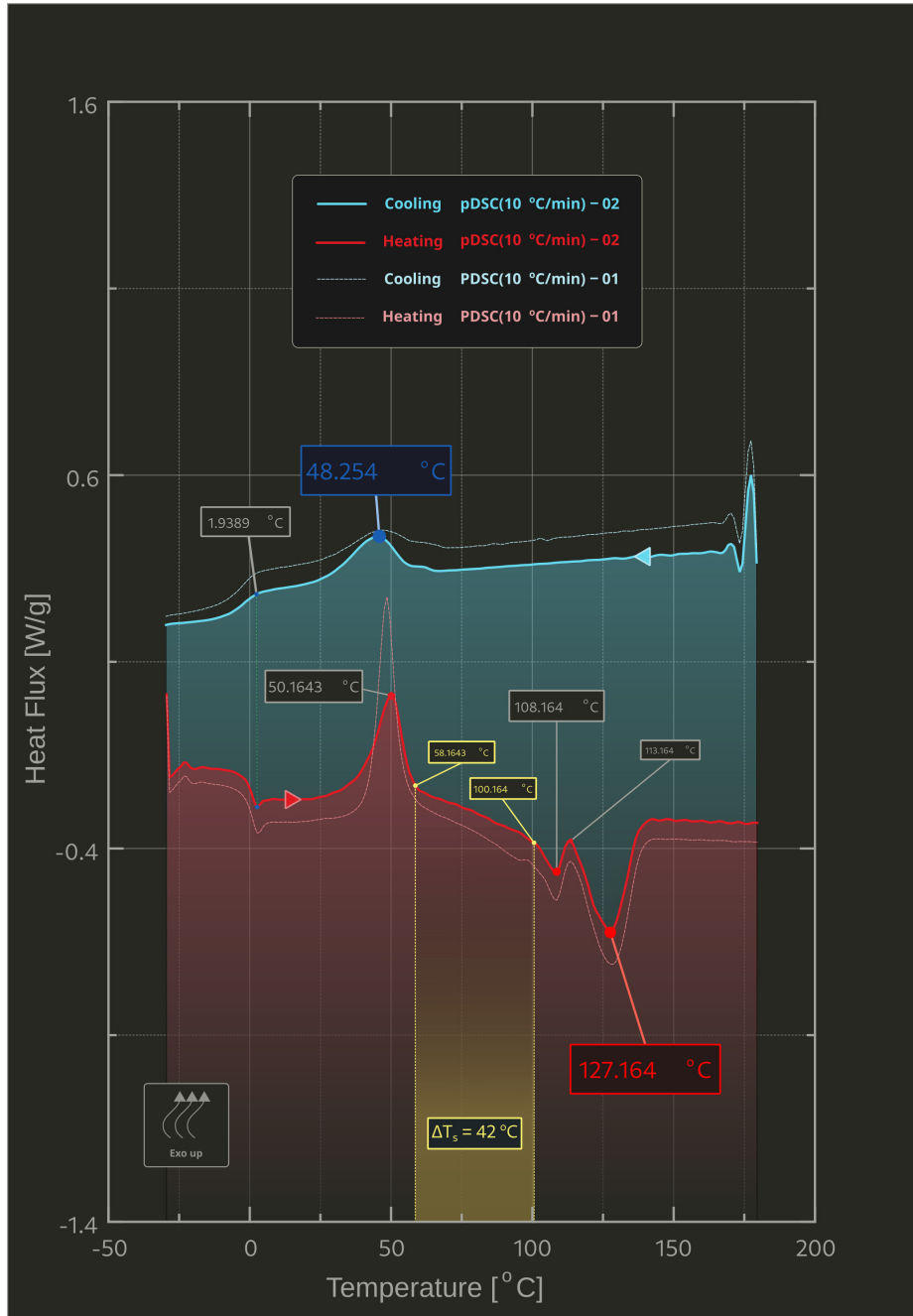


Figure 23: DSC analysis of PHBH at 10 $^{\circ}$ C/min

The plot highlights a consistent behaviour and only minor differences between the powder and pellet samples, with the powder specimen showing a slightly wider sintering window, which is a very desirable trait for SLS, as explained in previous chapters (6.1, 3.1.1) and in accordance with the available literature [8, 27, 7].

As evident from the heating phase (23), the powder sample shows a main peak melting point of $T_m = 127.164\text{ }^{\circ}\text{C}$, with a secondary melting point of $T_m = 108.164\text{ }^{\circ}\text{C}$, as well as a crystallization point at $T_c = 50.1643\text{ }^{\circ}\text{C}$. The cooling phase highlights a main peak crystallization point of $T_c = 48.254\text{ }^{\circ}\text{C}$ as well, indicating that the main crystallization activity occurs around that temperature range in both phases.

A minor peak activity is also observed at around $2\text{ }^{\circ}\text{C}$ in both the heating and cooling phases (with a more prominent peak during heating), and this can be attributed to the glass transition temperature of the polymer, which can be further investigated using a DMA (17).

The powder sample data has been used to calculate the enthalpy values around the two main crystallization peaks and the main melting peak, with the following approach:

- The heat flux data points are normalized by the specimen weight, which does not have a data set of its own from the DSC test, but can be assumed to be constant within the temperature range, which is a resonable assumption based on the TGA results (12.2)
- The normalized heat flow is then plotted against time for both the heating and cooling phases and a line is hand drawn around the peaks
- The area between the peaks and the base line represents an estimate of the enthalpy value

The enthalpy values are then calculated using the following equation, which is solved numerically:

$$\Delta H = \int_{t_0}^{t_1} \phi(t) dt \quad [J/g] \quad (5)$$

where $\phi(t)$ is the normalized heat flow and t_0 and t_1 are the time values at which the line is drawn.

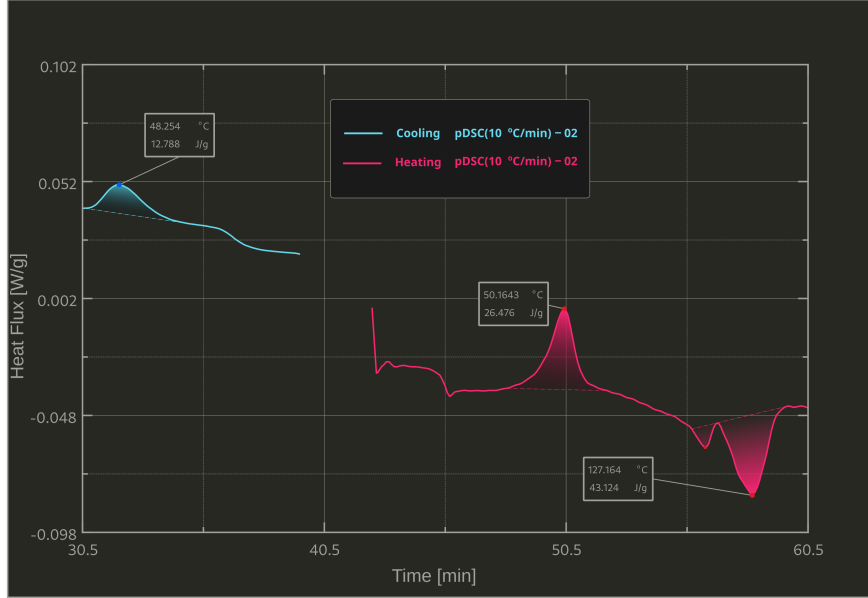


Figure 24: Enthalpy values for the DSC analysis of PHBH at 10 °C/min

The obtained enthalpy values can be used to derive the estimated percentage of crystallinity of the material, using the following equation:

$$X_c = \frac{\Delta H_m - \Delta H_{cc}}{\Delta H_m^0 \cdot m} \quad [\%] \quad (6)$$

where ΔH_m is the enthalpy value of the melting peak, ΔH_{cc} is the enthalpy value of the cold crystallization peak, m is the mass of the specimen and ΔH_m^0 is the enthalpy value of the melting peak of a pure crystalline material, which is 146 J/g for PHBH [12].

All the highlighted temperatures and other relevant quantities are summarized in the following table:

ID	ΔH_c [J/g]	T_c^{peak} [°C]	T_g [°C]	T_{cc}^{peak} [°C]	ΔH_{cc} [J/g]	ΔH_m [J/g]	T_{m1}^{onset} [°C]	T_{m1}^{peak} [°C]	T_{m2}^{onset} [°C]	T_{m2}^{peak} [°C]	X_c [%]
PDSC	10.633	48.687	2.087	49.117	34.847	48.753	103.022	107.990	110.579	128.554	11.281
pDSC	12.788	48.254	1.939	50.164	26.476	43.124	100.164	108.164	113.164	127.164	14.555

Table 3: Results of the DSC analysis showcasing phase transition points, enthalpies and crystallinity of the material

12.2 TGA (Thermal Gravimetric Analysis)

Thermal Gravimetric Analysis is a technique that constantly measures the mass of an object subjected to a deliberate change in temperature for a certain period of time through a precision scale.

Time, temperature and mass are the involved variables and while mass is a direct measure, whose sudden changes (visible peaks in the weight vs temperature plot) can indicate relevant transition points, time and temperature are directly controlled as machine parameters.

Generally speaking, TGA instruments can be set up for different workflows:

- static or isothermal analysis, where weight changes are registered over a specified time frame, at a fixed temperature of interest
- quasi-static analysis, where temperature is changed in discrete steps, with isothermal intervals in between
- dynamic analysis, where temperature is changed in a continuous linear fashion

The analysis can be set up to end after a certain time, temperature or residual weight and be performed in vacuum, air or inert gas such as argon.

This analysis technique can be used to reveal many important temperature values where physical transformations or chemical reactions occur, pinpoint the presence of certain materials with known transition points, in samples of unknown composition, (e.g residual moisture can be detected by checking any sudden weight changes around 100 °C, water's boiling point), determine the complete degradation cycle of a sample, testing the thermal stability of a material at its operational temperature, etc.

12.2.1 Results

The analysis has been firstly performed on the raw pellet material, as a benchmark test that consistently returned the expected degradation behaviour, over multiple analysis.

The test has then been conducted on powder samples and SLS printed samples, focusing on finding relevant discrepancies with the reference behaviour, which could potentially highlight the presence of impurities that might have been undetected during SEM analysis ([11.2](#)).

The TGA analysis was performed on a *Mettler-Toledo TGA/SDTA 851e* [30] instrument, in air atmosphere, with a heating rate of 10 °C/min and a temperature range of 25 °C to 900 °C.



Figure 25: Mettler-Toledo TGA/SDTA 851e [30]

The specimens that have undergone a TGA analysis have been assigned an ID with the following criteria:

$$ID = x - TGA_{NN} \quad (7)$$

where x is the specimen type (pellet, powder or sintered), TGA is the analysis type and NN is the sample number.

The specimens have been catalogued in the following table:

ID	Type	Weight [mg]
$P - TGA_{01}$	pellet	29.0641
$p - TGA_{02}$	powder	15.4821
$p - TGA_{03}$	powder	38.2253
$s - TGA_{04}$	sintered	10.5330

Table 4: TGA specimens

The analysis data has been exported with *Mettler-Toledo's* included software [30] (12.1), after normalizing the data to the initial weight of the sample, then

imported, elaborated and plotted with *Labplot* [14].

The following figures show the results of the TGA analysis on the pellet, powder and sintered samples.

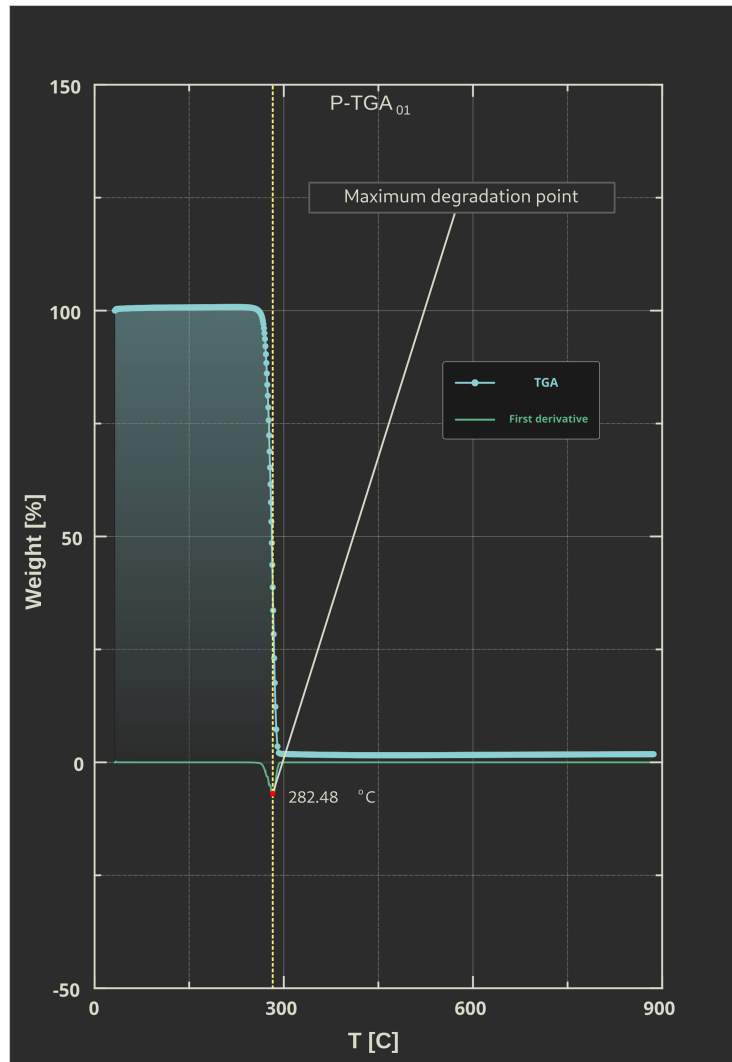


Figure 26: TGA analysis of pellet sample $P - TGA_{01}$ (4)

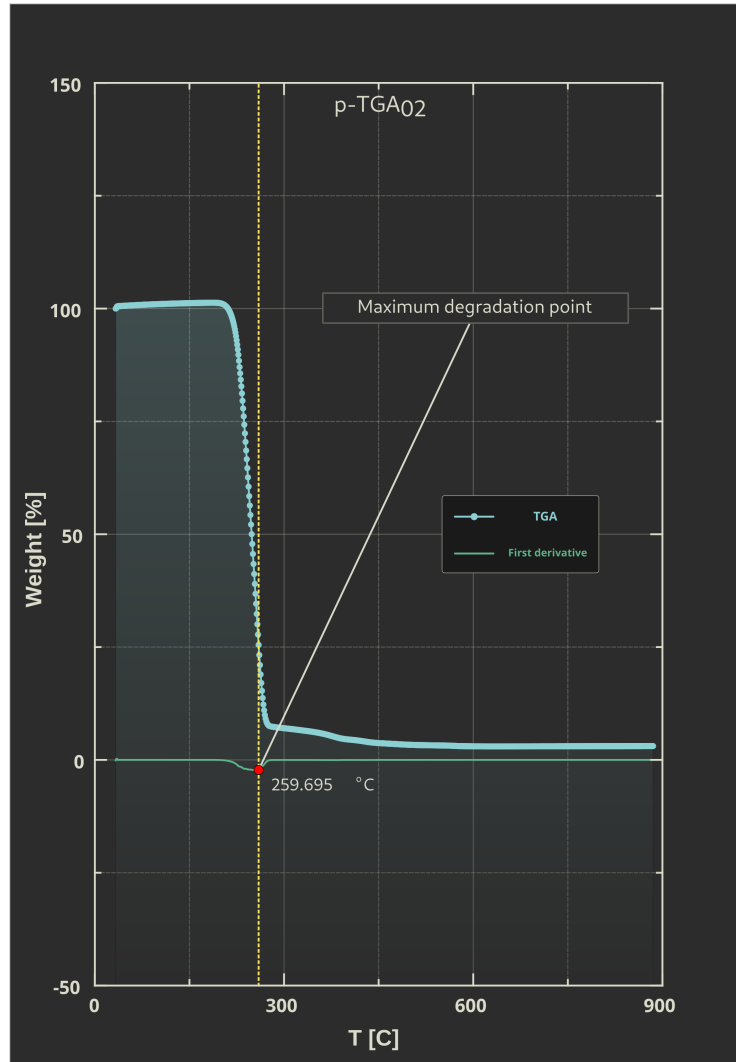


Figure 27: TGA analysis of powder sample $p-TGA_{02}$ (4)

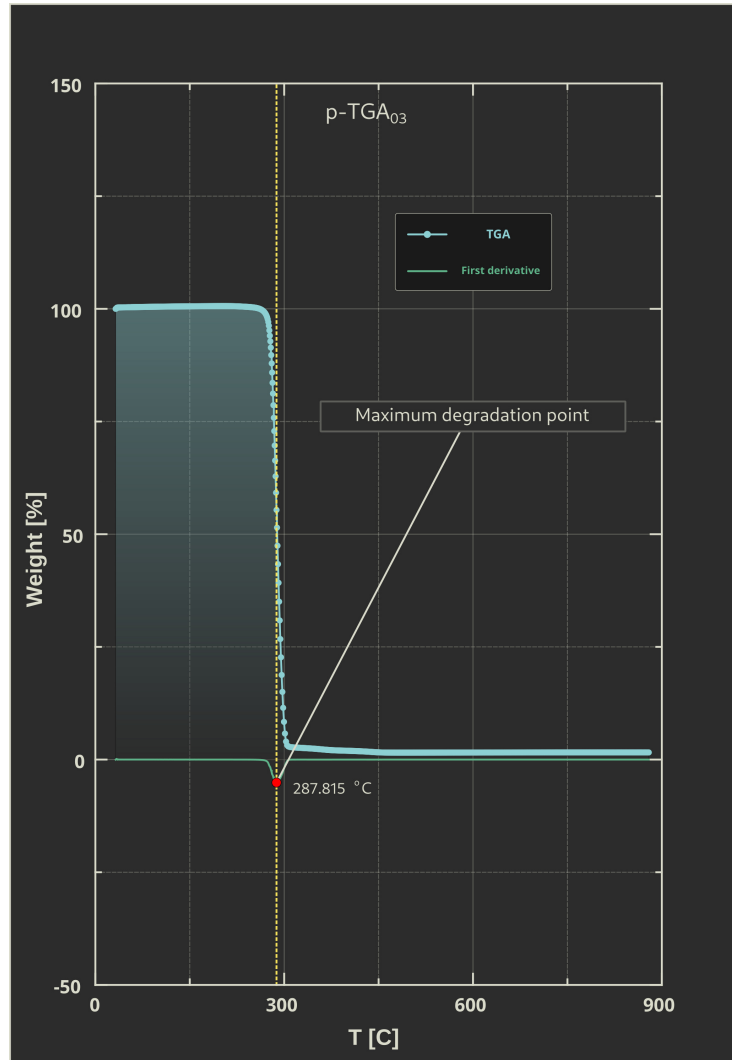


Figure 28: TGA analysis of powder sample $p - \text{TGA}_{03}$ (4)

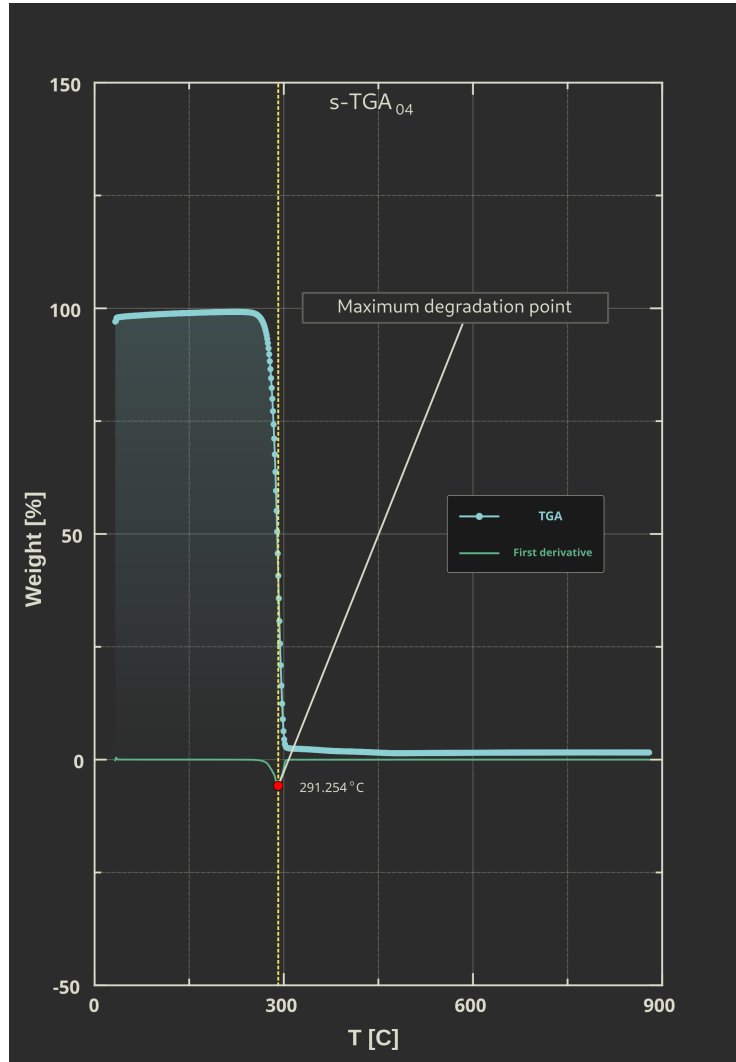


Figure 29: TGA analysis of sintered sample $s - TGA_{04}$ (4)

The results of the TGA analysis showcase the expected thermal behaviour of the powder and sintered samples, which are consistent with the pellet sample.

The TGA curves show an exponentially increasing weight loss, with very similar slopes, and the additional first derivative showcases a consistent behaviour among all samples, with clear degradation peaks at approximately the same temperature values.

13 Density measurement

The true density of the powder is an important parameter to determine its flowability, which is a key factor in the SLS printing process, as better described in (14).

Its value should be ideally identical to the theoretical density of the material, which is stated to be 1.20 kg/m^3 in its datasheet [18].

The density of the powder has been measured with a *Ultrapyc 5000 gas pycnometer* [20].



Figure 30: Ultrapyc 5000 gas pycnometer [20]

A 0.626 g sample of the powder has been weighed and placed in the sample cell, then the pycnometer has been filled with helium gas and the measurements have been performed at 20°C , using the *pulse* preparation and the *fine powder* flow rate presets available in the device settings.

The test has been iterated with a total of 15 steps, with a 0.01% precision and three measurements per pass, giving an average density value of 1.213602 kg/m^3 , consistent with the expected theoretical value.

14 Flowability analysis

The flowability of a powder is a key factor in the success of the SLS process, as it impacts the way the powder is deposited on the build platform. Some powders are more prone to clumping, which can lead to the formation of bridges between the powder particles, which can cause the build platform to become clogged and the build to fail.

A powder with a good flowability will be able to flow freely and evenly, without clumping, and will be able to fill the build platform evenly, without leaving any gaps.

Powders with poor flowability can be improved by adding a flowability agent, which can be a lubricant, a binder or a combination of both.

The flowability of a powder can be tested by performing a flowability analysis, which can be performed in a number of ways, depending on the standard that is being followed.

The analysis has been performed on the powder samples, using the *tap density* method, which is the most common approximation test, as described by ASTM D7481 [4].

The standard describes how to evaluate the packing factor and the Hausner Ratio of a powder sample (that needs to be dried, before being tested, as residual moisture negatively impacts the flowability), using a 100 mL graduated cylinder, following the steps described for procedure *b*.

The Hausner Ratio is evaluated with the equation described in previous chapters (1, 6.1), and the packing factor is evaluated with the following equation:

$$\varphi = \frac{\rho_{bulk}}{\rho} \quad (8)$$

where ρ_{bulk} is the bulk density and ρ is the true material density.

As previously mentioned in (6.1) and according to the available literature, the Hausner Ratio of the powder should be ideally below 1.4 [27], which is consistent with the experimental findings.

15 Granulometry analysis

The granulometry analysis has been performed on an oven dried powder sample, using a *Malvern Morphologi 4* [22].



Figure 31: Malvern Morphologi 4 [22]

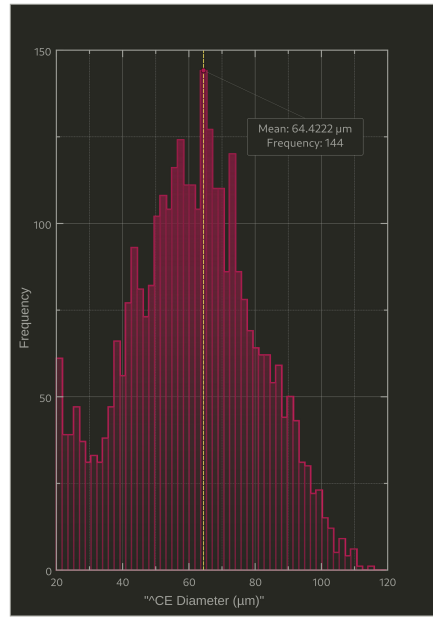
The sample has been measured in terms of volume, with a 5 mm^3 specimen being spread on a glass plate in the most homogeneous way possible, by using a 4 bar dispersion pressure and a 10 ms injection time.

An homogenous powder distribution is crucial in order to avoid particle overlap and to obtain a more accurate representation of the powder granulometry.

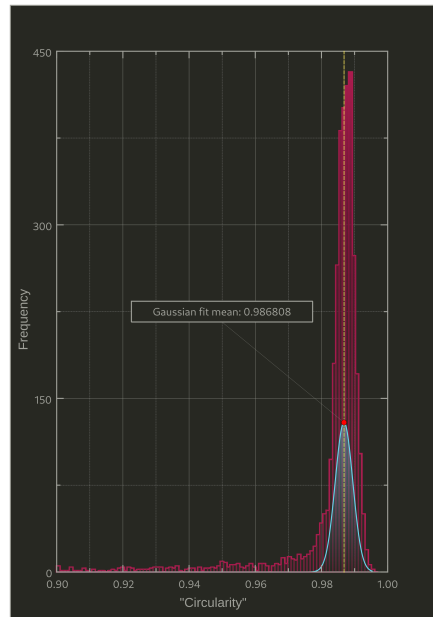
The instrument has taken several images of the powder specimen, using a 10X magnification, and by z-stacking images with different focal lengths, in order to achieve better results.

All particles below $20 \mu\text{m}$ have been excluded from the analysis, which has been performed by using an automated static imaging algorithm, performed by the instrument's software.

The output results have been analyzed and the most meaningful features have been plotted using *Labplot* [14].



(a) Particle Size Distribution



(b) Particle Circularity Distribution

Figure 32: Granulometry analysis of the powder sample

The results of the granulometry analysis showcase particle sizes compatible with SLS powder requirements (6.1), as well as a great particle circularity distribution, which is consistent with the findings of the SEM analysis (11.2.1).

The average particle diameter is $64.4222 \mu m$, with a count of 144 over a total of more than 3000 analyzed particles (32a).

The average circularity is extremely close to a perfectly spherical shape, with a mean value of roughly 0.98 (32b).

16 SLS printing

After the powder has been characterized, the next step is to print it with the SLS machine.

Before being printed, the powder can be mixed with a small quantity of a binder, to improve the flowability of the powder. However, given the excellent flowability of the PHBH powder (14), this step has been skipped.

The next preparation step is to further dry the powder, in order to remove any residual moisture that could have accumulated during the storage period, and to homogenize the powder distribution by shaking the container for a few minutes.



Figure 33: SLS ready powder batch

16.1 Print files preparation

The next step is to prepare the print files, which are the files that will be sent to the SLS machine, to instruct it on how to print the part.

The approach can vary depending on the software used to prepare the files, but the general idea is to create a 3D model of the part, then slice it into layers, and finally export the files to the SLS machine.

The pipeline starts with the creation of a 3D model of the part and ends with a g-code file, and can be summarized as follows:

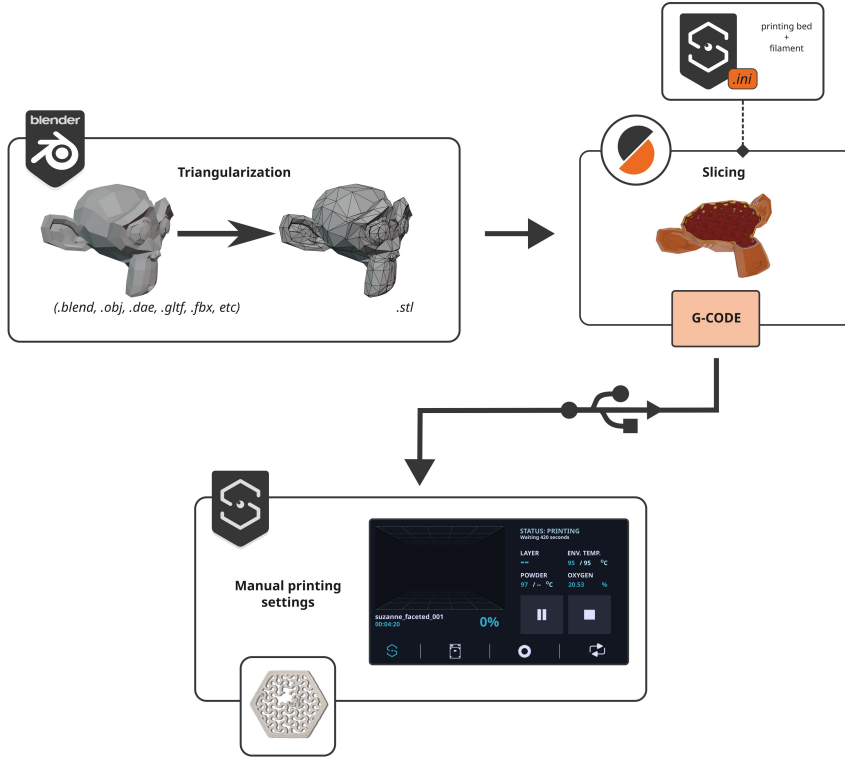


Figure 34: 3D printing file pipeline

16.1.1 3D model creation

The first step is to create a 3D model of the part, which can be done in many ways, depending on the software used.

The models have been created from scratch, either by directly modeling them in *Blender* 3.3.1 [10], or by creating SVG files in *Inkscape* 1.2 [23] and then extruding them in *Blender*, where they are handled as bezier curves.

This approach is particularly useful for this case study, where planar complex geometries better suit the SLS printing process with low powder availability and low printing volumes. As seen in (16.3), the SLS printed parts are extremely small, with heights in the order of millimeters.

Working with planar geometries also allows to easily create very intricate 3D

models, by simply extruding the 2D SVG file, which as earlier mentioned is handled as bezier curves and inherits their properties, such as resolution dependant smoothness, non destructive extrusion and custom profile beveling.

The extruded bezier curves have then been converted to meshes, remeshed when necessary, and finally exported as STL files (which is the most common file format for 3D printing), using Blender's internal 3D Printing Toolbox addon, which also offers useful mesh stats and automatic mesh fixing tools.

16.1.2 Slicing

The next step is to slice the 3D model into layers, which is done by the slicing software.

The slicing software takes the STL file as input (or other formats such as OBJ, which are automatically triangulated during the import), and outputs a g-code file, which is the file that will be sent to the SLS machine.

There are some caveats with slicing software, which are worth mentioning.

The first one is that the software is not able to handle meshes with non manifold edges, so the STL file must be checked for non manifold edges before being imported.

More importantly, all slicing software is designed to work with an FDM workflow, whereas many industrial SLS machines tend to have a dedicated CNC software.

This means that the slicing software is not able to handle the SLS workflow without workarounds.

The most common workaround is to load a custom configuration file for the slicing software, which will instruct it on how to handle the SLS workflow for a specific printer. The slicing software is not aware of the SLS workflow, so it will slice the model based on a FDM workflow, and the custom configuration file, which bundles a set of parameters for the printing area and a fictitious filament.

While clearly there is no filament extrusion in SLS, once the software has sliced the model by simulating an FDM workflow, the output g-code file will be compatible with the SLS machine and provide accurate movement instruction.

The slicing software used for this case study is *PrusaSlicer* [25], which is a free and open source slicing software, forked from the *Slic3r* project.

The SLS machine used for this case study does not have a dedicated CNC software, but the manufacturer provides a custom *.ini* bundle configuration file for *PrusaSlicer*, which is a universal file format, and can be used by any slicing

software.

16.2 Sharebot Snowwhite²

The SLS machine used for this case study is the *Sharebot Snowwhite²*, which is an open hardware and open source desktop SLS machine, designed by the italian company *Sharebot* [26].



Figure 35: Sharebot Snowwhite²

The system is very modular and it features a standard powder distributor with a working area of 100x100x100 mm, but a reduced distributor with a 20x40x60 mm area has been used, given the available quantity of PHBH powder.

The printer utilizes a CO₂ laser with a 14 W maximum power output and a 10.6 μm wavelength. Power is controlled as a percentage of its maximum output. A value of 25 % has been generally set for solid pieces, whereas a 30-35 % range is preferred for pieces with extremely thin walls and intricate structures. The power for the border has been set to a 5 % increment with respect to the inner layers.

The printer features a user friendly touch screen GUI, but all its features and

logs can be accessed remotely for further control from any terminal. The printer is equipped with a 3D camera, which allows to monitor the printing process in real time, and to take pictures of the printed parts at every layer.

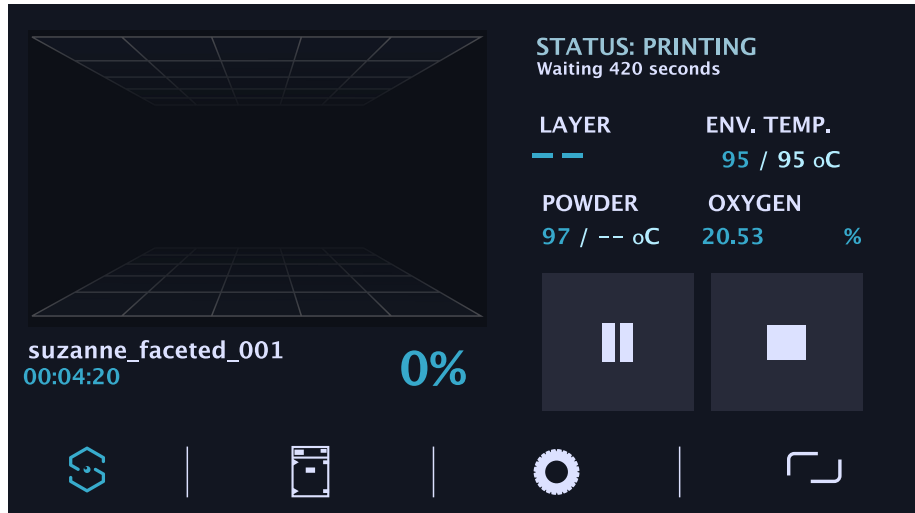


Figure 36: Sharebot Snowwhite² UI

The polymer powder is distributed by a blade recoater, but a roller option is also available. Air has been used for the printing process, but nitrogen or argon can be fed through the chamber, should a modified atmosphere be needed.

The printer is also equipped with a powder recovery system, which allows to recover the powder after the printing process, and to reuse it for further prints.

The environment temperature has been set in a range of 85-95 °C, with variable rates of success, whereas values outside this threshold showcased critical issues, i.e. high porosity, sheeting and delamination at low temperatures or adhesion to the recoater and consequent destruction of the printed specimen.

Another configurable variable is laser hatching speed, which is measured relative to machine resolution, in dots/s, which corresponds to 0.06 mm/s in metric units.

This has generally been kept at default values (40000 dots/s for the inner layers and 64000 dots/s for the border).

A maximum of three warming layers has been used for these prints, i.e. the powder is raised and warmed up for three layers, without any laser hatching, to allow the powder to settle and to avoid powder sheeting.

A higher number of warming layers might be needed for larger prints, but it has

not been tested ([16.1.1](#)).

Once the environment temperature has been set in the desired range (ideally within the theoretical sintering window), the printer ramps it up in gradual steps, until the target is reached. An additional waiting time of 120-300 s has been set after reaching the desired temperature, in order to let heat uniformly distribute through the powder bed.

The tank offset has been set prior to printing, depending on the desired print height or layer number, which is calculated with the following formula:

$$Z = \frac{1}{2} \cdot (0.3 N) \quad [mm] \quad (9)$$

where:

- Z is the tank offset, in mm
- N is the number of layers to be printed
- 0.3 is the layer height, in mm, which is the default value for the *Sharebot Snowwhite*²
- $\frac{1}{2}$ is a correction factor, which is needed to account for the fact that the printing area is fed powder from two side tanks.

16.3 Printed samples

Given the experimental nature of this work, several samples have been printed, with gradual increases in complexity, in order to test the limits of the SLS workflow for the novel material.

As earlier mentioned (16.2), the printer is modular and despite being equipped with a default 100x100x100 mm working area, a reduced distributor with a 20x40x60 mm area has been used, given the available quantity of PHBH powder.

This setup is ideal for small scale prints, but as it will be shown later, the current results are not exhaustively representative of the potential of the SLS workflow for PHBH.

There are in fact intrinsic limitations to extremely small objects with intricate and fine details, especially at low z-height, which are related to both the material itself (as it is fragile and prone to breaking) and the printing resolution of the SLS machine, which did not seem to be able to print extremely small features with high fidelity to the original models.

These limitations become less and less relevant with increasing z-height, as the part becomes more robust, as well as with increasing overall size, where the printing resolution is able to catch finer details with better accuracy.

Nonetheless, the current results are still very promising, and they showcase the potential of the SLS workflow for PHBH, which can be further explored with larger prints, where the complexity of the models can be pushed even further, as expected with SLS technology.

The first samples are simple geometries, which have been printed to test the feasibility of the SLS workflow for PHBH. Square and rectangular prisms have been printed, with different z-heights, starting from single layers, up to 15 layers, as a baseline for the following tests.

The initial goal was in fact to find adequate printing parameters for the material, which required a lot of trial and error, as the material is very sensitive to the printing conditions.

The first prints have been made with a 25 % laser power setting, which has been found to be a reasonable value for solid pieces, by visual inspection of single layers (which showcased decent densification) and later confirmed by mechanical testing on multilayer samples.

Some of the initial samples are showcased in the following figure:



Figure 37: First printing attempts. Porosity and defects are more visible in the single layer samples. The rectangular prisms were the first to showcase a good level of densification and lack of deformation and have been used as a baseline for the following tests.

As previously mentioned, the material is very sensitive to the printing conditions, and other than laser power, the environment temperature has been found to be the most critical parameter.

After a long series of tests, the optimal temperature range has been found to be $85^{\circ}\text{C} - 95^{\circ}\text{C}$, which has been used for the following tests.

It is important to note that the environment temperature is measured by a thermocouple, whereas the powder bed temperature (which is a few degrees higher) is measured by an infrared sensor, which is less accurate. Therefore, these values might vary slightly for different machines, depending on how the different temperatures are measured.

The next step was to test the material with more complex geometries, which have been printed with the same temperature range, but with a 30-35 % laser power setting, which has been found to be optimal for the emptier geometries, where heat is dissipated more easily, given the lower thermal mass.

When dealing with thin, hollow and complex geometries, the most prominent issue is the tendency of the blade recoater to stick to the printed piece and wipe the part out, which is a common issue with SLS technology, and which can be caused by different factors, such as the powder bed temperature, the laser power, the environment temperature, the powder type and the powder distribution, among the many.

Given the multifactorial and complex nature of the aforementioned issue, it is not possible to pinpoint the exact cause of the problem, but it is possible to find a compromise between the different parameters, which allows for a successful print.

The introduction of other settings such as warming layers, pre-print and between-layers waiting time, has been found to be useful in order to avoid the blade recoater from wiping the part out.

Using a roller recoater might also be a solution, but it has not been tested.

The following printed specimens have been modeled as mentioned in (16.1.1) and have been catalogued with the following criteria:

$$NN - filename_{type} \quad (10)$$

where:

NN is the number of layers and the type is either *filled* or *thin* for densely filled and hollow geometries, respectively.

ID	Type	Layers	Bounding box size [mm]	Laser power [%]	Environment temperature [$^{\circ}\text{C}$]
15 - dragonlogofilled	Filled	15	22x15.69x2	25	90
15 - hexagonfilled	Filled	15	30x30x2	25	95
55 - octagonholesthin	Thin walls	55	30x30x8	35	95
01 - squarefilled	Filled	01	20x20x0.15	25	85
50 - boatthin	Thin walls	50	40x15x7	30	90
10 - DMA01filled	Filled	10	30x10x1	25	90
15 - DMA02filled	Filled	15	50x10x1	25	90
15 - organicpatternthin	Thin walls	15	30x30x2	35	87

Table 5: A list of the most relevant 3D printed specimens

The selected specimens are showcased in the following figures:

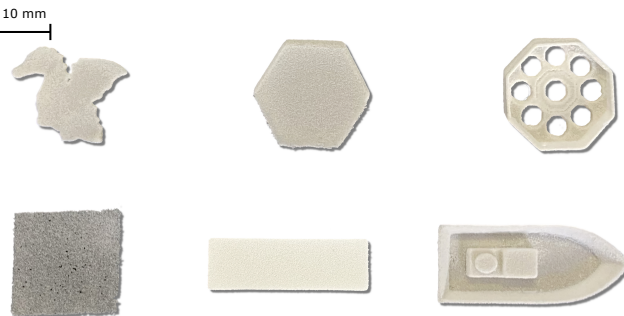


Figure 38: From top to bottom, clockwise: 15 - *dragonlogofilled*, 15 - *hexagonfilled*, 55 - *octagonholesthin*, 50 - *boatthin*, 10 - *DMA01filled*, 01 - *squarefilled* (5).

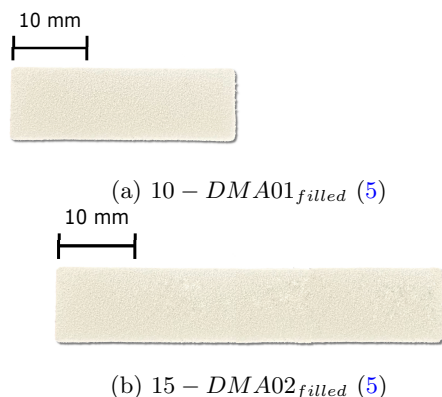
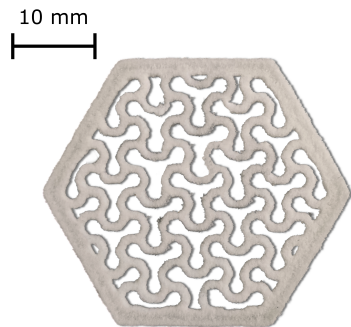
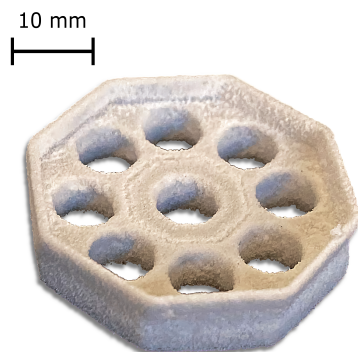


Figure 39: Printed specimens used for DMA testing.



(a) 15 – *organicpatternthin*, showcasing an intricate organic pattern (5).



(b) 55 – *octagonholesthin*, showcasing an octagon with a circular array of octagon holes (5).

Figure 40: Printed specimens with complex internal patterns.

17 Dynamic Mechanical Analysis

A non-destructive DMA has been used to determine some of the mechanical properties of SLS printed PHBH. The analysis allows for the determination of the storage modulus E' , the loss modulus E'' as well as the $\tan\delta$, which is the ratio between the loss modulus and the storage modulus.

As mentioned in (12.1), the DMA can also be used to better determine the glass transition temperature T_g , which has been initially estimated to be around $2\text{ }^{\circ}\text{C}$ by the DSC analysis of a PHBH powder sample (23). However, the revealed peak activity in that temperature range can not be attributed to the glass transition in a definitive way, by means of a DSC analysis alone.

The glass transition temperature, which is defined as the temperature at which the material changes from a glassy to a rubbery state, (i.e. the temperature at which the material changes its stress-strain behavior from brittle to plastic), can be determined with better precision by a DMA.

More specifically, the transition point can be revealed by a prominent peak in the $\tan\delta$ curve, indicating a sudden change in the moduli ratio of the material.

The analysis has been performed with a Triton Technology DMA instrument [16], on the SLS sample 10 – $DMA01_{filled}$ that has been printed specifically for the purpose of the DMA analysis (16, 5, 39).

The test has been run with an oscillating uniaxial stress amplitude of 1 N, at a frequency of 1 Hz, with an initial chamber temperature of $-77.7\text{ }^{\circ}\text{C}$ (achieved by cooling the environment with liquid nitrogen), and has been stopped once the sample reached the rubbery plateau, i.e. a temperature region below the melting point, in which the material exhibits an almost constant modulus behaviour [9].

The results of the DMA analysis are shown in the following figure, where the $\tan\delta$ curve has been upscaled significantly in order to match a relative scale with the other curves.

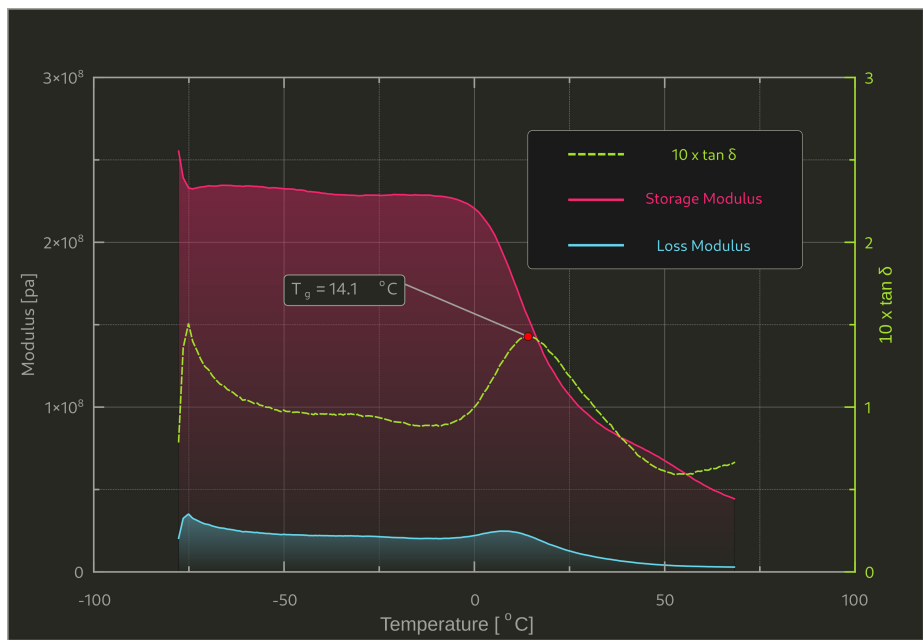


Figure 41: DMA analysis of the SLS sample 10 – $DMA01_{filled}$ (5).

The $\tan\delta$ curve (41) shows a clear peak at $14.1\text{ }^{\circ}\text{C}$, which is the glass transition temperature of the material, in disaccordance with the initial estimation of $2\text{ }^{\circ}\text{C}$ (23).

As expected for a polymer of the PHA family, both the storage modulus E' and the loss modulus E'' are very low, in line with the typical viscoelastic behavior of all biopolymers [15], which are not suited for structural applications and are instead used for packaging and other non-structural applications, such as biomedical implants and scaffolds [11].

Unsurprisingly, the mechanical properties of the material fall behind those of typical SLS polymers, which can occasionally reach storage moduli a whole order of magnitude higher than that of PHBH, according to this DMA.

That in itself is not a major issue, as SLS parts are not limited to structural applications or mechanical pieces: other properties, such as biodegradability, biocompatibility and low toxicity can be very desirable traits in a wide range of applications.

Moreover, the mechanical and thermal properties of the material can be improved by adding fillers, creating blends with other biopolymers or creating composites with other materials.

Given the successful SLS printability, with unaltered thermal properties among the raw material, the powder and the printed parts (as highlighted by the TGA and DSC analysis results (12.2, 12.1)), as well as mechanical properties that meet the expected behavior of a bioplastic, PHBH is a very promising polymer that can further enrich the catalogue of sustainable materials available for additive manufacturing.

18 Future development and research

The entire project has been carried out with an experimental approach and, despite poor direct support from the currently available literature, a better understanding of the material and its behavior has emerged, but the need for further research and development is still present.

Starting from the powder production pipeline, the results have already been excellent ([10](#), [9](#), [10.4](#)) with the available notions and tools, bringing the pellet to powder yield to a very significant increase.

However, the process is still in its infancy, and the entire premise of the project is to develop a sustainable and cost-effective production pipeline, which is not only able to produce a high-quality powder, but also to do so in a way that is environmentally friendly. Therefore, the next step is to find a way to reproduce and even improve the results obtained with the current recipe, but in a more sustainable way, by further investigating the use of alternative solvents.

Another possibility is to find a way to retrieve the evaporated chloroform, assuming an effective solvent recovery system is available and cost-effective.

The next step is to further investigate the use of the powder in the SLS process, by further optimizing the printing parameters, the powder granulometry and morphology and experimenting with different additives or material blends that could improve the mechanical properties of the material, as well as investigating the possibility of enhancing the printed parts with post-processing techniques.

References

- [1] Gomez Bonilla; Dechet M.A.; Schmidt J.; Peukert W.; Buck A. “Thermal rounding of micron-sized polymer particles in a downer reactor: direct vs indirect heating”. In: *Rapid Prototyping Journal* 26.9 (2020).
- [2] Open AI. *DALL-E 2*. 2022. URL: <https://labs.openai.com>.
- [3] Open AI. *Round particles seen through a SEM microscope*. 2022. URL: <https://labs.openai.com/e/8rNkMtCHXwQmVW0GZ00sc20q/ZCX0rjp8yxNf2UvDrupbdSuW>.
- [4] ASTM. *Standard Test Methods for Determining Loose and Tapped Bulk Densities of Powders using a Graduated Cylinder*. en. Standard ASTM D7481 18. 2018. URL: <https://compass.astm.org/document/?contentCode=ASTM%7CD7481-18%7Cen-US>.
- [5] Federico Lupone; Elisa Padovano; Francesco Casamento; Claudio Badini. “Process Phenomena and Material Properties in Selective Laser Sintering of Polymers: A Review”. In: *Materials* (2021).
- [6] Kaneka Biopolymers. *PHBH*. 2022. URL: <https://kanekabiopolymers.com/phbh-applications/>.
- [7] Maximilian A Dechet and Jochen Schmidt. “On the Development of Polymer Particles for Laser Powder Bed Fusion via Precipitation”. eng. In: *Procedia CIRP* 94 (2020), pp. 95–99. ISSN: 2212-8271.
- [8] Kerim Eraslan et al. “Poly(3-hydroxybutyrate-co-3-hydroxyhexanoate) (PHBH): Synthesis, properties, and applications - A review”. In: *European Polymer Journal* 167 (2022), p. 111044. ISSN: 0014-3057. DOI: <https://doi.org/10.1016/j.eurpolymj.2022.111044>. URL: <https://www.sciencedirect.com/science/article/pii/S0014305722000489>.
- [9] J.D. Ferry. *Viscoelastic Properties of Polymers*. 3rd. New York: John Wiley & Sons, 1980.
- [10] Blender Foundation. *Blender*. 2022. URL: <https://www.blender.org>.
- [11] Alberto Giubilini et al. “Advantages of Additive Manufacturing for Biomedical Applications of Polyhydroxyalkanoates”. In: *Bioengineering* 8.2 (2021). ISSN: 2306-5354. DOI: [10.3390/bioengineering8020029](https://doi.org/10.3390/bioengineering8020029). URL: <https://www.mdpi.com/2306-5354/8/2/29>.
- [12] J. Ivorra-Martinez et al. “Development and characterization of sustainable composites from bacterial polyester poly(3-hydroxybutyrate-co-3-hydroxyhexanoate) and almond shell flour by reactive extrusion with oligomers of lactic acid”. English. In: *Polymers* 12.5 (2020). Cited By :12. URL: www.scopus.com.
- [13] Jiao Jian, Zeng Xiangbin, and Huang Xianbo. “An overview on synthesis, properties and applications of poly(butylene-adipate-co-terephthalate)-PBAT”. In: *Advanced Industrial and Engineering Polymer Research* 3.1 (2020), pp. 19–26. ISSN: 2542-5048. DOI: <https://doi.org/10.1016/j.aiepr.2020.01.001>. URL: <https://www.sciencedirect.com/science/article/pii/S2542504820300014>.

- [14] KDE. *Labplot*. 2022. URL: <https://labplot.kde.org>.
- [15] Adriana Kovalcik. “Recent Advances in 3D Printing of Polyhydroxyalkanoates: A Review”. In: *The EuroBiotech Journal* 5 (2021).
- [16] Triton Technology Ltd. *Triton-Lacerta Technology*. 2022. URL: <https://www.lacerta-technology.com>.
- [17] Hemantkumar Junghare*; Mayur Hamjade; C.K.Patil; S.B.Girase; Mandar M.Lele. “A Review on Cryogenic Grinding”. In: *International Journal of Current Engineering and Technology* (2017).
- [18] Gruppo Maip. *Gruppo Maip*. 10036 Settimo Torinese (TO), Italy, 2022. URL: www.maipsrl.com.
- [19] FRITSCH Milling and Sizing. *Cryogenic Grinding with the Variable Speed Rotor Mill PULVERISETTE 14 premium line*. <https://www.youtube.com/watch?v=3KUGXICL3Is>. 2021.
- [20] Anton Paar. *Ultrapyc 5000 Gaspycnometer*. 2022. URL: <https://www.anton-paar.com/corp-en/products/details/ultrapyc/>.
- [21] Øyvind Kolås; Jehan Pagès and many others. *GNU Image Manipulation Program*. <https://www.gimp.org>.
- [22] Malvern Panalytical. *Malvern Morphologi 4*. Malvern Panalytical, Malvern, Worcestershire, UK, 2022. URL: <https://www.malvernpanalytical.com/en/products/product-range/morphologi-range/morphologi-4>.
- [23] The Inkscape Project. *Inkscape*. <https://inkscape.org>.
- [24] S. Ayu Rafiqah et al. “A Review on Properties and Application of Bio-Based Poly(Butylene Succinate)”. In: *Polymers* 13.9 (2021). ISSN: 2073-4360. DOI: [10.3390/polym13091436](https://doi.org/10.3390/polym13091436). URL: <https://www.mdpi.com/2073-4360/13/9/1436>.
- [25] Prusa Research. *PrusaSlicer*. 2022. URL: <https://www.prusa3d.com>.
- [26] Sharebot S.r.l. *Sharebot*. 2022. URL: <https://www.sharebot.it/en/>.
- [27] Manfred Schmid, Antonio Amado, and Konrad Wegener. “Polymer powders for selective laser sintering (SLS)”. In: *AIP Conference Proceedings* 1664.1 (2015), p. 160009. DOI: [10.1063/1.4918516](https://doi.org/10.1063/1.4918516). eprint: <https://aip.scitation.org/doi/pdf/10.1063/1.4918516>. URL: <https://aip.scitation.org/doi/abs/10.1063/1.4918516>.
- [28] Pixelmator Team. *Pixelmator Pro*. 2022. URL: <https://www.pixelmator.com/pro/>.
- [29] Tescan. *FIB-SEM, TESCAN S9000G, Tescan*. 2018. URL: <https://www.tescan.com/fib-sem-tomography-of-biological-specimens-with-the-new-tescan-s9000g/#file-lead?filename=Advanced-Focused-Ion-Beam-Scanning-Electron-Microscopy-for-3D-ultrastructural-analysis-of-mitochondria-ER-in>.
- [30] Mettler Toledo. *Mettler Toledo*. 2022. URL: <https://www.mt.com>.

- [31] Lisa Jiaying Tan; Wei Zhu; Kun Zhou. “Recent Progress on Polymer Materials for Additive Manufacturing”. In: *Advanced Functional Materials* (2020).